CALIFORNIA INSTITUTE OF TECHNOLOGY

MATERIALS SCIENCE

W. M. KECK LABORATORY OF ENGINEERING MATERIALS

PASADENA

When U. S. Government drawings, specifications, or other data are used for any purpose other than a definitely related Government procurement operation, the Government thereby incurs no responsibility nor any obligation whatsoever, and the fact that the Government may have formulated, furnished, or in any way supplied the said drawings, specifications, or other data, is not to be regarded by implication or otherwise, or in any manner licensing the holder or any other person or corporation, or conveying any rights or permission to manufacture, use, or sell any patented invention that may in any way be related thereto.

MATSCIT PS 66-2

MATERIALS SCIENCE

CALIFORNIA INSTITUTE OF TECHNOLOGY

POLYMER SCIENCE REPORT

PHYSICOMECHANICAL BEHAVIOR OF RUBBERLIKE MATERIALS

P. J. Blatz

AFRPL-TR-66-22 JANUARY 1966

Second Annual Report

2 February 1965 - 31 January 1966

Contract Number AF 04(611)-9572
Program Structure Number 750G
AFSC Project Number 3059

Air Force Rocket Propulsion Laboratory
Research and Technology Division
Edwards Air Force Base, California
Air Force Systems Command
United States Air Force

W. M. Keck

Laboratory of Engineering Materials

Pasadena, California

PREFACE

The primary goal of these studies is the understanding of the response and failure behavior of filled rubberlike materials.

Failure data are being accumulated in uniaxial, biaxial, and triaxial stress fields as functions of temperature and load level. Times-to-break in each stress field are being measured and interpreted in terms of a stochastic model. This approach is leading to a general failure criterion which is expected to be of use in determining mechanical failure of rocket motors.

Response behavior is being interpreted in terms of sedimentation theory and strain energy formulations. The application of each of these approaches depends upon extension of current theories.

ABSTRACT

During the past year, further progress was made in understanding both the molecular nature of the strain energy function of a homogeneous, nearly incompressible rubberlike material. The importance of non-affinity of deformation, chain stiffness, and volume exclusion in modifying the basic statistical model of Kuhn, Grün, James and Guth are discussed.

A phenomenological theory for predicting the distribution of times-to-break arising in creep failure in terms of the growth of defects in rubber was proposed and showed good agreement with experimental data.

Batches of thermoelastic rubber filled with glass beads are being prepared prior to evaluation in terms of sedimentation theory.

TABLE OF CONTENTS

SECTION		PAGE
I	MECHANICAL BEHAVIOR OF GUM RUBBER VULCANIZATES	1
	A. MOLECULAR BASIS FOR RUBBERLIKE ELASTICITY	1
	1. Nature of Rubberlike Elasticity	1
	2. Excluded Volume	2
	3. Internal Energy Effects	5
	4. Chain Entanglements	5
	5. Non-affine Deformation and Chain Stiffness	5
	B. THERMOMECHANICS OF RUBBERLIKE ELASTICITY	16
	C. CREEP FAILURE OF GUM RUBBER VULCANIZATES	22
	1. Introduction	22
	2. Stochastic Theory of Defects in Rubber Vulcanizates	25
	3. Relation Between Crack Rate and Stress Field	40
	4. Distribution of Break Times	42
	D. TENSILE BEHAVIOR OF SWOLLEN AND UNSWOLLEN GUM RUBBER VULCANIZATES	48
	1. Statistical Analysis of Ring Dimensions	48
	2. Effect of Solvents Upon the Mechanical Behavior of the Kawabata Formulation	50
	3. Swelling of Rings in Toluene	51
	4. Solvent Treatment of the Kawabata Formulation	53
	5. Optimization Studies on SBR-MBT and SBR-MBTS Formulations	54
	E. CHEMICAL ANALYSIS OF SULFUR IN MILLED MASTER BATCHES AND GUM VULCANIZATE	55
	1. Introduction	55
	2. Analytical Results	56
II	PHYSICOMECHANICAL BEHAVIOR OF FILLED GUM RUBBER VULCANIZATES	57
	A. INTRODUCTION	57
	REFERENCES	58
	FIGURES	59
	TABLES	84

TABLE OF FIGURES

FIGURE		PAGE
1	Mooney-Rivlin Plot for Non-Affine Deformation of 2-Link Chain.	59
2	Break Stress-Break Time Data Determined by T. Smith.	60
3	Break Stress-Break Time Data Determined by J. Halpin.	61
4	Break-time — Break-load Correlation for Creep Failure Data on SBR at 75°F.	62
5	Crack Rates Calculated from First and Second Moments of Break-time Distribution.	63
6	Break-time Distribution as a Function of Mean Break Time: Master Check of Break-Time Theory.	64
7	Correlation between Mean Break Time in Creep and True Stress Level in Simple Tension.	65
8	Area-Weight Correlation.	66
9	Thickness-Weight Correlation.	67
10	Width-Weight Correlation.	68
11	SBR-MBT-S Unswollen.	69
12	SBR-MBT-S Swollen in Toluene, Vacuum Dried.	70
13	SBR-MBT-S Swollen in Toluene, Acetone Extracted.	71
14	SBR-MBT-S, Acetone Extracted.	72
15	Weight-Thickness Correlation from Traveling Microscope	73
16	Mooney-Rivlin Plot for SBR-MBTS Swollen in Toluene, and Pulled at 1"/min Dripping Wet.	74
17	Mooney-Rivlin Plot for SBR-MBTS Swollen in Toluene, Vacuum Dried, Acetone Extracted, and Pulled at 1"/min Dripping Wet.	75
18	Mooney-Rivlin Plot for SBR-MBTS Acetone Extracted, and Pulled Dripping Wet.	76
19	Mooney-Rivlin Parameters as a Function of Solvent Treatment at +24°C.	77
20	Mooney-Rivlin Parameters as a Function of Solvent Treatment at -24°C.	78

FIGURE		PAGE
21	Time Dependence of Swelling of SBR-MBTS Ring in Toluene at Room Temperature.	79
22	Ultimate Properties of Plasticized Kawabata Formulations Pulled at +24°C for Various Cure Schedules and Various Curative Concentrations Based on MBT.	80
23	Ultimate Properties of Plasticized Kawabata Formulations Pulled at +24°C for Various Cure Schedules and Various Curative Concentrations Based on MBTS.	81
24	Ultimate Properties of Plasticized Kawabata Formulations Pulled at -30°C for Various Cure Schedules and Various Curative Concentrations Based on MBT.	82
25	Ultimate Properties of Plasticized Kawabata Formulations Pulled at -30°C for Various Cure Schedules and Various Curative Concentrations Based on MBTS.	83

TABLE OF TABLES

TABLE		PAGE
I	Mean Break Time and Crack Growth Rates as a Function of Load.	84
II	Mooney-Rivlin Patameters for SBR-MBT-S Vulcanizates	85

I. MECHANICAL BEHAVIOR OF GUM RUBBER VULCANIZATES

A. MOLECULAR BASIS FOR RUBBERLIKE ELASTICITY

1. Nature of Rubberlike Elasticity

It is now well established that most of the force field engendered in a well-cured rubber network subjected to a deformation field arises from the change in the number of configurations available to the polymer chains. If the number of available configurations in the deformed state is less than that of the undeformed state the polymer chain is in tension, and vice versa. If one neglects completely all interactions between chains, and assumes that each chain is completely flexible and is composed of n freely rotating statistical segments, each of length ℓ, one calculates that the probability density that the tail of the undeformed chain has coordinates $\{m = \frac{r}{\ell}, \theta, \varphi\}$ relative to the head is given by:

$$\Phi_n(m,\theta,\varphi) = \frac{q\left(\frac{sh}{q}\, e^{-q\mathcal{L}}\right)^n}{(2\pi n)^{3/2}\, \mathcal{L}\sqrt{(1/q^2) - (1/sh^2)}} \tag{1}$$

where

$$\mathcal{L} \equiv cth - \frac{1}{q} = \frac{m}{n} \tag{2}$$

$$q = \mathcal{L}^{-1}\left(\frac{m}{n}\right) \tag{3}$$

$$sh \equiv \sinh q \tag{4}$$

$$cth \equiv \text{ctnh } q \tag{5}$$

Equation (1) is obtained by the method of steepest descents and is exact in the limit $m \to 0$. On the other hand, in the limit $m \to n$, the exact expression is given by:

$$\Phi_n(m,\theta,\varphi) \Rightarrow \left(\frac{sh}{q}\ e^{-q\mathfrak{L}}\right)^n \qquad (6)$$

which is not very different from (1) for $n \gg 2$.

When equation (1) was used to fit simple tensile data obtained on an SBR vulcanizate, it was found that n may be as low as 7, in which case (1) should be replaced by (6). More important however is the fact that (1) and/or (6) represents the data, as plotted in the form $\frac{\sigma}{\lambda-\frac{1}{\lambda^2}}$ vs $\frac{1}{\lambda}$, the so-called Mooney-Rivlin plot, only for $\lambda > \sim 2$. In other words, the slope of the Mooney-Rivlin curve predicted by (1) and/or (6) is always negative. The above statistical function does not predict the softening of the vulcanizate during initial stretch.

There are several possible reasons for this phenomenon which are not accounted for in the model. They are:

a. excluded volume

b. internal energy effects

c. chain stiffness

d. non-affine deformation

e. chain entanglements.

We shall comment at various lengths on each of these possibilities.

2. Excluded Volume

In a recent publication, Edwards[1] has shown that the effect of excluded volume is to bias the Gaussian approximation of (1) toward larger average end-to-end distances. Thus, if the Gaussian approximation to (1) is given by:

$$\Phi_{nG} = \left(\frac{3}{2\pi n}\right)^{3/2} e^{-\frac{3}{2}\frac{m^2}{n}} \tag{7}$$

then Edwards' expression is given by:

$$\Phi_{nE} = \frac{\alpha^3}{2\pi^{3/2}\beta + 4\pi\beta + \pi^{3/2}} e^{-(\alpha r - \beta)^2}, \quad r \geq \beta \tag{8}$$

where

$$\alpha^2 = \frac{3^3}{2^2 \times 5\, n\ell^2} \tag{9}$$

and

$$\beta^{10} = \frac{3^9 \times 5\, nv^2}{2^{10}\pi^2\ell^6} \tag{10}$$

and where v is the excluded volume. Equation (8) is normalized to unity, from it, we immediately calculate:

$$\alpha\langle r\rangle = \int_\beta^\infty r \times \Phi_{nE}\, 4\pi r^2\, dr = \frac{\beta^3\sqrt{\pi} + 3\beta^2 + \frac{3\beta}{2}\sqrt{\pi} + 1}{\sqrt{\pi}\,\beta^2 + 2\beta + \frac{\sqrt{\pi}}{2}} \tag{11}$$

$$\alpha^2\langle r^2\rangle = \int_\beta^\infty r^2 \times \Phi_{nE}\, 4\pi r^2 dr = \frac{\sqrt{\pi}\,\beta^4 + 4\beta^3 + 3\sqrt{\pi}\beta^2 + 4\beta + \frac{3}{4}\sqrt{\pi}}{\sqrt{\pi}\,\beta^2 + 2\beta + \frac{\sqrt{\pi}}{2}} \tag{12}$$

There are two things immediately questionable about the Edwards' expression. One is the significance of the lower limit of r. It implies that the chain can not touch head-to-tail much like a person who can not touch his toes. If conversely, the lower limit is taken to be zero, formulae (11) and (12) are replaced by much more involved expressions containing incomplete gamma functions. In either event, and this is the second point, in the limit $\beta \to 0$,

(11) and (12) do not reduce to their Gaussian equivalents. Thus the Edwards' expression needs reworking.

Before undertaking this task, it is worthwhile to ask whether the concept of excluded volume produces a probability density function (8) which predicts the correct shape of the Mooney-Rivlin plot. We have examined this question for the special case of simple tension applied to an incompressible network and arrive at the result:

$$\frac{\sigma\lambda}{NkT} = \frac{2}{3}\alpha^2\langle r^2\rangle\left(\lambda^2 - \frac{1}{\lambda}\right) + \beta\alpha\langle r\rangle F(\lambda) \tag{13}$$

where

$$F(\lambda) = \frac{(4\lambda^3 - 1)\,\ell n\left(\lambda^{3/2} + \sqrt{\lambda^3 - 1}\right)}{2\sqrt{\lambda}\,(\lambda^3 - 1)^{3/2}} - \frac{(2\lambda^3 + 1)\,\lambda}{2(\lambda^3 - 1)} \tag{14}$$

In the limit $\lambda \to 1$, we find that:

$$\frac{d\mu_{n\ell}}{d\left(\frac{1}{\lambda}\right)} \equiv \frac{d\left(\frac{\sigma}{\lambda - \frac{1}{\lambda^2}}\right)}{d\left(\frac{1}{\lambda}\right)} \to -NkT\,\frac{64}{105}\,\beta\alpha\langle r\rangle \tag{15}$$

Thus the slope of the excluded volume function is negative, can be shown to be negative for all λ, and reduces to zero when there is no excluded volume. Thus, it is not worthwhile to investigate further the effect of excluded volume. This is not to say that the concept of excluded volume is not a meaningful one, but rather that it does not at this stage provide the next most important feature that the model needs, namely the initial softening of the nonlinear modulus $\mu_{n\ell}$ with increasing strain.

3. Internal Energy Effects

Internal energy effects will be discussed in the next chapter of this section. On the basis of what was shown in the preceding annual report, it is readily observed that internal energy effects would not be expected to change the shape of the Mooney-Rivlin plot.

4. Chain Entanglements

No realistic model of chain topology including entanglements is currently available. This maybe an important acquisition to the statistical model. We plan to investigate the formalization of this concept later on.

5. Non-affine Deformation and Chain Stiffness

As pointed out in paragraph A. 1., the number of statistical segments needed to fit tensile data out to the point of break is relatively small, ~ 7. With this in mind, we first decided to investigate the form of the rigorous expression for a freely rotating chain composed of only two links and to compare this with the form predicted by (1) and/or (6) when n is set equal to 2. Some surprising things develop which lead us to investigate separately the effects of non-affine deformation and chain stiffness.

We recall that the probability that the terminus of a link have spherical coordinates $\{ \theta, \varphi \}$ relative to its origin is given by:

$$dp_1 = \frac{\sin \theta_1 \, \Delta\varphi_1 \Delta\theta_1}{4\pi} \tag{16}$$

where $\{ \Delta\varphi_1, \Delta\theta_1 \}$ are the angular measures of the edges of any incremental spherical quadrangle on the surface of a sphere bonded by: $\{ 0 \leq \theta_1 \leq \pi, 0 \leq \varphi_1 \leq 2\pi \}$.

The combined probability that the terminus of the first link have spherical coordinates $\{ \theta_1, \varphi_1 \}$ and that of the second link relation to its origin have spherical coordinates $\{ \theta_2, \varphi_2 \}$ is given by:

$$dp_{12} = \frac{\sin\theta_1 \Delta\varphi_1 \Delta\theta_1}{4\pi} \times \frac{\sin\theta_2 \Delta\varphi_2 \Delta\theta_2}{4\pi} \tag{17}$$

Let us now introduce new coordinates $\{\beta;\ m,\ \theta,\ \varphi\}$ to replace the old coordinates $\{\theta_1\ \varphi_1\ ;\ \theta_2\ \varphi_2\}$, where $\{m,\ \theta,\ \varphi\}$ are the spherical coordinates of the terminus of the second link relative to the origin of the first link, and where β is the angle of rotation of the joint of the chain in the plane normal to the radius vector $\vec{m}$. This arrangement is shown in the sketch below.

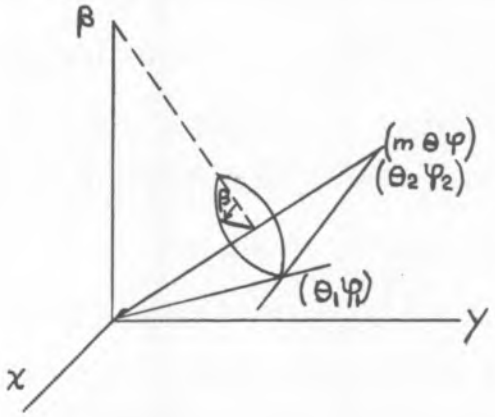

Using the new variable β, the probability that the terminus of the second link have spherical coordinates $\{m,\ \theta,\ \varphi\}$ relative to the origin of the first link and regardless of the configuration of the joint is then given by:

$$dp_2 \equiv \oint_\beta \frac{\sin\theta_1\, d\varphi_1\, d\theta_1}{4\pi} \frac{\sin\theta_2\, d\varphi_2\, d\theta_2}{4\pi} \tag{18}$$

Before evaluating (18) let us compare it with the statistical expression which leads to (1) and/or (6). For general n, the analogue of (18) is given by:

$$\Phi_n = \sum n! \prod_i \prod_j \frac{\left(\frac{\sin\theta_i \Delta\varphi_i \Delta\theta_i}{4\pi}\right)^{n_{ij}}}{n_{ij}!} \qquad (19)$$

$$\Sigma\Sigma n_{ij} = n$$

$$\Sigma\Sigma n_{ij} \sin\theta_i \cos\varphi_j = m \sin\theta\cos\varphi$$

$$\Sigma\Sigma n_{ij} \sin\theta_i \sin\varphi_j = m \sin\theta\sin\varphi$$

$$\Sigma\Sigma n_{ij} \cos\theta_j = m \cos\theta$$

For the case $n = 2$, the n_{ij}'s can only be two 1's with remaining 0's, except for the case where the chain is completely stretched out, in which case one of the n_{ij}'s is 2 and all the other zero.

Thus the restrictor summations become, for the case of bent chain:

$$1 + 1 + 0 + 0 + 0 + \cdots\cdots = 2 \qquad (20)$$

$$\sin\theta_1 \cos\varphi_1 + \sin\theta_2 \cos\varphi_2 = m \sin\theta\cos\varphi \qquad (21)$$

$$\sin\theta_1 \sin\varphi_1 + \sin\theta_2 \sin\varphi_2 = m \sin\theta\sin\varphi \qquad (22)$$

$$\cos\theta_1 + \cos\theta_2 = m \cos\varphi \qquad (23)$$

The combinatorial function is given by:

$$\frac{n!}{\pi\pi n_{ij}!} \doteq \frac{2!}{1!\ 1!\ 0!\ 0!\ 0!\ \cdots\cdot} \doteq 2 \qquad (24)$$

Now the restrictor summation (20) is an identity and thus really provides no restriction. Equations (21, 22, and 23) determine $\{\varphi_1\ \varphi_2$ and $\theta_2\}$ in terms of $\{\theta_1; m_1\ \theta_1\ \varphi\}$. Thus the combined restriction is equivalent to summing over allowable values of θ_1. Thus (19) becomes in the limit:

$$\Phi_2 = 2 \int_{\theta_1} \frac{\sin\theta_1 d\varphi_1\, d\theta_1}{4\pi} \frac{\sin\theta_2 d\varphi_2\, d\theta_2}{4\pi} \qquad (25)$$

which is identical with (18), because for each value of θ_1 there are <u>two</u> allowable values of φ_1 and/or θ_2. Thus integrating from the lower limit of θ_1 to its upper limit (cf sketch)

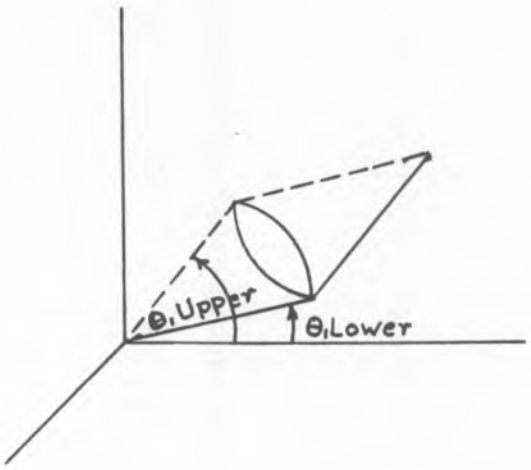

is equivalent to integrating with respect to β from 0 to π or from $-\pi$ to 0. The statistical factor 2 weights the contour properly.

Thus (19) should give the same result as (18) with n = 2. The fact is however that it does not! The reason for this is as follows. Equation (19) is converted by use of the multinomial theorem to:

$$\Phi_n = \text{coeff } u^m \sin\theta\cos\varphi \; v^m \sin\theta \sin\varphi \; w^m \cos\theta \; \text{in} \left(\int_0^{\pi} \oint \frac{\sin\theta' d\theta' d\varphi'}{4\pi} \, u^{\sin\theta'\cos\varphi'} \, v^{\sin\theta'\sin\varphi'} \, w^{\cos\theta'} \right)^n \tag{26}$$

This transformation is exact and is independent of $\underline{n}$. Next we evaluate the double integral to obtain:

$$\Phi_n = \text{coeff } u^m \sin\theta\cos\varphi \; v^m \sin\theta\sin\varphi \; w^m \cos\theta \; \text{in} \left(\frac{sh}{p} \right)^n \tag{27}$$

where

$$p = \sqrt{\ell n^2 u + \ell n^2 v + \ell n^2 w} \tag{28}$$

This transformation is exact and is independent of n. The coefficient of (27) is obtained formally by the triple residue of:

$$\Phi = \left(\frac{1}{2\pi i} \right)^3 \oint\oint\oint \frac{\left(\frac{sh}{p} \right)^n d\ell nu \, d\ell nv \, d\ell nw}{u^m \sin\theta\cos\varphi \; v^m \sin\theta\sin\varphi \; w^n \cos\theta} \tag{29}$$

Now, in evaluating (29), we used the method of steepest descents, which is really only good for either n very large or for a very peaked saddle on the real axis of the contour. It can be shown that the saddle is actually broad and shallow so that it is not a sufficiently good approximation to replace the integral of (29) by its second order approximation in a Taylor's expansion. More important however, it is easily shown that the radius of convergence of the Taylor's expansion decreases as $\underline{m}$ decreases, which corresponds in a loose sense to $\lambda \to 1$. Thus, no expansion of (29) yields a result which is valid for the unstretched chain, and a fortiori, which is valid for the strain energy as the stretch field approaches unity. So all this "scientific" wonderment through the past twenty years at the failure of the finite chain model to predict the correct sign of the so-called C_2 term in the Mooney-Rivlin plot has been without foundation. In other words, before ascribing the failure to other effects, it yet remains to determine the exact form of the probability function.

For general $\underline{n}$ this means a search for an alternative way of evaluating (25) which is exact, or for $n = 2$, this means the evaluation of (18) which is also exact. A fortiori, once (18) is evaluated, one can combine two two-link chains to make a four link chain and so on. Let us see where this path leads. First, we express $\{ \theta_1 \varphi_1 ; \theta_2 \varphi_2 \}$ in terms of $\{ \beta ; m \theta \varphi \}$ to obtain by simple trigonometry:

$$\cos \theta_{1,2} = \cos \chi \cos \theta \mp \sin \chi \sin \theta \cos \beta \tag{30}$$

$$\varphi_{1,2} = \varphi \mp \arctan \frac{\sin \chi \sin \beta}{\cos \chi \sin \theta \pm \sin \chi \cos \theta \cos \beta} \tag{31}$$

where

$$\cos \chi = m/2 \tag{32}$$

In terms of the new variables, (18) becomes:

$$dp_2 = \oint_\beta \frac{J \sin\theta_1 \sin\theta_2}{16\pi^2} \, d\beta d\varphi \, d\theta \, d\chi \tag{33}$$

where

$$J \equiv \left| \frac{\partial(\theta_1 \varphi_1 \theta_2 \varphi_2}{\partial(\beta \varphi \theta \chi)} \right| \tag{34}$$

After evaluating the determinant, one obtains:

$$J \sin\theta_1 \sin\theta_2 = 4 \sin\chi \cos\chi \sin\theta \tag{35}$$

so that:

$$dp_2 = \frac{\sin\chi \cos\chi \, d\chi}{2\pi} \sin\theta \, d\theta \, d\varphi \tag{36}$$

or

$$dp_2 = \frac{1}{8\pi m} m^2 \sin\theta d\varphi \, d\theta \, dm \tag{37}$$

After separating the differential element of volume in spherical coordinates, one obtains the probability density

$$\Phi_2 = 1/8\pi m \tag{38}$$

which is to be compared with the statistical function obtained by method of steepest descents:

$$\Phi_2 = \frac{q\left(\frac{sh}{q} e^{-q\mathcal{L}}\right)^2}{(4\pi)^{3/2} \mathcal{L} \sqrt{\frac{1}{q^2} - \frac{1}{sh^2}}} \tag{39}$$

which representation, we repeat, is only good for large m, i.e. as $m \to n = 2$. In this limit the exact expression (38) takes on the value $1/16\pi$ or $\sim 2\%$, and the representation (39) takes on the value $1/4^{5/2}\pi^{3/2}$ or $\sim 1\%$. Thus, as $m \to n$, the disparity between the two functions is not great. On the other hand, as $m \to 0$, the exact function becomes infinite, the representation (which now lies outside the radius of convergence of the expansion of the function which

engendered it) is given by

$$\left(\frac{3}{4\pi}\right)^{3/2} e^{-\frac{3m^2}{4}} \rightarrow \left(\frac{3}{4\pi}\right)^{3/2} ,$$

which is finite. Thus one should expect radically different stress behavior at small stretch ratios from the exact function.

The entropy of a chain whose radial probability function is given by (37) is given by:

$$\frac{s_{ch}}{k} = \ell n \left(\frac{1}{8\pi m} \cdot m^2 \sin\theta \, d\varphi \, d\theta \, dm\right) \tag{40}$$

If the end of this chain is moved, the new coordinates are given by:

$$\frac{x'}{\ell} = m' \sin\theta' \cos\varphi' = \lambda_1 \, m \sin\theta \cos\varphi \tag{41}$$

$$\frac{y'}{\ell} = m' \sin\theta' \sin\varphi' = \lambda_2 \, m \sin\theta \sin\varphi \tag{42}$$

$$\frac{z'}{\ell} = m' \cos\theta' = \lambda_3 \, m \cos\theta \tag{43}$$

Equivalently one has:

$$m' = m \sqrt{\lambda_1^2 \sin^2\theta \cos^2\varphi + \lambda_2^2 \sin^2\theta \sin^2\varphi + \lambda_3^2 \cos^2\theta} \tag{44}$$

$$\tan\theta' = \frac{\sqrt{\lambda_1^2 + \lambda_2^2}}{\lambda_3} \tan\theta \tag{45}$$

and

$$\tan\varphi' = \frac{\lambda_2}{\lambda_1} \tan\varphi \tag{46}$$

The entropy of the deformed chain is given by:

$$\frac{s'_{ch}}{k} = \ell n \left(\frac{1}{8\pi m} \bullet m'^2 \sin\theta' d\varphi' d\theta' dm' \right) \tag{47}$$

which upon introducing (44-46) becomes:

$$\frac{s'_{ch}}{k} = \ell n \left(\frac{\sqrt{I_3}\ m^2 \sin\theta d\varphi d\theta dm}{8\pi m \sqrt{\lambda_1^2 \sin^2\theta\cos^2\varphi + \lambda_2^2 \sin^2\theta \sin^2\varphi + \lambda_3^2 \cos^2\theta}} \right) \tag{48}$$

where

$$\sqrt{I_3} \equiv \lambda_1 \lambda_2 \lambda_3 = \left| \frac{\partial(m'\theta'\varphi')}{\partial(m\ \theta\varphi)} \right| \tag{49}$$

Assuming incompressibility and no internal energy change the entropy change or strain energy (w) associated with the deformation of a chain is given by:

$$\frac{s_{ch} - s'_{ch}}{k} \equiv - \frac{\Delta s_{ch}}{k} \equiv - \frac{T\Delta s_{ch}}{kT} = \frac{w_{ch}}{kT} = \ell n \left(\frac{m'}{m} \right) \tag{50}$$

Assuming that the network entropy is an additive function of the individual chain entropies, the total entropy change is given by:

$$\frac{W}{NkT} = \int_{\substack{\text{conf.} \\ \text{space}}} \ell n \left(\frac{m'}{m} \right) dp_2 \tag{51}$$

Now in all the previous published work on the statistical theory of rubber elasticity, investigators have assumed an affine deformation, even though such a situation cannot possibly be accepted by even the most hypothetical of all networks. The reason for this is simple. Of all the chains in the network, there will be a certain fraction which are completely or nearly completely stretched out. For such chains the maximum increase in end-to-end distance which is measured by $\left(\sqrt{\lambda_1^2 + \lambda_2^2 + \lambda_3^2} - \sqrt{3} \right)$ cannot be very

large, say ten percent, just for the sake of argument. Thus, if the invariant ($I_1 \equiv \lambda_1^2 + \lambda_2^2 + \lambda_3^2$) exceeds $1.1 \times \sqrt{3}$, these particular chains will either snap or else cause a force readjustment among other chains resulting in a non-affine deformation field. We are forced to consider the latter possibility. In the particular case n = 2, the maximum value of $m' = 2$, so that m can never exceed

$$m \leq \frac{2}{\sqrt{\lambda_1^2 \sin^2\theta\cos^2\varphi + d_2^2 \sin^2\theta\sin^2\varphi + \lambda_3^2\cos^2\theta}} \tag{52}$$

Thus (51) must be evaluated as:

$$\frac{W}{NkT} = \frac{1}{2}\int_0^{\pi}\oint\int_0^{\frac{2}{\sqrt{\lambda_1^2\sin^2\theta\cos^2\varphi+\lambda_2^2\sin^2\theta\sin^2\varphi+\lambda_3^2\cos^2\theta}}}$$

$$\ell n\left(\lambda_1^2\sin^2\theta\cos^2\varphi + \lambda_2^2\sin^2\theta\sin^2\varphi + \lambda_3^2\cos^2\theta\right)\frac{m\sin\theta\,d\varphi\,d\theta\,dm}{8\pi}$$

$$+\int_0^{\pi}\oint\int_{\frac{2}{\sqrt{\lambda_1^2\sin^2\theta\cos^2\varphi+\lambda_2^2\sin^2\theta\sin^2\varphi+\lambda_3^2\cos^2\theta}}}^{2}$$

$$\ell n\left(\frac{2}{m}\right)\frac{m\sin\theta\,d\varphi\,d\theta\,dm}{8\pi} \tag{53}$$

Upon simplification (53) becomes:

$$\frac{W}{NkT} = \int_0^{\pi}\sin\theta\,d\theta\oint\frac{d\varphi}{8\pi}\left[1 - \frac{1}{\lambda_1^2\sin^2\theta\cos^2\varphi + \lambda_2^2\sin^2\theta\sin^2\varphi + \lambda_3^2\cos^2\theta}\right] \tag{54}$$

$$= \frac{1}{2} - \frac{1}{4}\int_0^{\pi}\frac{\sin\theta\,d\theta}{\sqrt{(\lambda_3^2\cos^2\varphi+\lambda_1^2\sin^2\theta)(\lambda_3^2\cos^2\varphi+\lambda_2^2\sin^2\theta)}} \tag{55}$$

$$= \frac{1}{2} - \frac{1}{2} \int_0^1 \frac{dx}{\sqrt{[\lambda_1^2 + (\lambda_3^2 - \lambda_1^2)\, x^2][\lambda_2^2 + (\lambda_3^2 - \lambda_2^2)\, x^2]}} \tag{56}$$

$$\frac{W}{NkT} = \frac{1}{2} - \frac{1}{2\lambda_2\sqrt{\lambda_3^2 - \lambda_1^2}}\, F\left[tn^{-1}\left(\frac{\sqrt{\lambda_3^2 - \lambda_1^2}}{\lambda_1} \right), \frac{\lambda_3\sqrt{\lambda_2^2 - \lambda_1^2}}{\lambda_2\sqrt{\lambda_3^2 - \lambda_1^2}} \right] \tag{57}$$

where

$$F(\varphi, k) = \int_0^{\varphi} \frac{d\vartheta}{\sqrt{1 - k^2 \sin^2\vartheta}} \tag{58}$$

and

$$tn^{-1}(\tan\varphi, k) = F(\varphi, k) \tag{59}$$

Alternatively (51) may be rewritten:

$$\frac{W}{NkT} = \frac{1}{2} - \frac{1}{2\lambda_2\sqrt{\lambda_3^2 - \lambda_1^2}} \times$$

$$F\left\{ F\left[\tan^{-1}\frac{\sqrt{\lambda_3^2 - \lambda_1^2}}{\lambda_1}, \frac{\lambda_3\sqrt{\lambda_2^2 - \lambda_1^2}}{\lambda_2\sqrt{\lambda_3^2 - \lambda_1^2}} \right], \frac{\lambda_3\sqrt{\lambda_2^2 - \lambda_1^2}}{\lambda_2\sqrt{\lambda_3^2 - \lambda_1^2}} \right\} \tag{60}$$

Equation (60) is the exact expression for the strain energy resulting from the non-affine deformation of a network of non-interacting chains each composed of two freely rotating links. It may be recast in terms of the stretch invariants by recalling that:

$$I_1 = \lambda_1^2 + \lambda_2^2 + \lambda_3^2 = \lambda_1^2 + \lambda_2^2 + \frac{1}{\lambda_1^2\lambda_2^2} \tag{61}$$

$$I_2 = (1/\lambda_1^2) + (1/\lambda_2^2) + (1/\lambda_3^2) = (1/\lambda_1^2) + (1/\lambda_2^2) + \lambda_{12}\lambda_2^2 \tag{62}$$

$$I_3 = \lambda_1^2\lambda_2^2\lambda_3^2 = 1 \tag{63}$$

After simplification, (61-63) can be reduced to:

$$\lambda_3^6 - I_1 \lambda_3^4 + I_2 \lambda_3^2 - 1 = 0 \tag{64}$$

which is the Cayley-Hamilton equation for an incompressible deformation. Thus we can write formally:

$$\lambda_3^2 = C_3(I_1 I_2) \tag{65}$$

$$\lambda_2^2 = \frac{(I_1 - C_3) + \sqrt{(I_1 - C_3)^2 - 4/C_3}}{2} \tag{66}$$

$$\lambda_1^2 = \frac{(I_1 - C_3) - \sqrt{(I_1 - C_3)^2 - 4/C_3}}{2} \tag{67}$$

where C_3 is any one of the real roots of the cubic equation.

We are now in a position to compute the stress components by differentiating (60). It is easier to return to (60), differentiate it, and then evaluate the integral, for the special case $\lambda_1 = \lambda_2 = 1/\sqrt{\lambda}$. This results in:

$$\frac{\sigma}{NkT} = \frac{1}{4}\left[\frac{(\lambda^3 + 2)\arctan\sqrt{\lambda^3 - 1}}{(\lambda^3 - 1)^{3/2}} - \frac{3}{\lambda^3 - 1}\right] \tag{68}$$

For small strains, (68) takes on the form:

$$\frac{\sigma}{NkT} = \frac{\lambda^3 - 1}{15} = \frac{\epsilon}{5} \tag{69}$$

Thus:

$$E = \frac{NkT}{5} \tag{70}$$

On the other hand, as $\lambda \to \infty$, $\sigma \to 0$. Thus (68) predicts the correct sign of the initial slope of the Mooney-Rivlin plot (cf Figure 1) but does not predict

the upswing with large strain, in fact does not predict a limiting strain. In order to explain this, it will be necessary to provide a more detailed analysis of chain interaction. In other words, the completely stretched out chains pull along the other chains and change their probability distribution. An analysis of this situation will be presented in a later technical report. The value of the limiting slope of the Mooney-Rivlin plot of (68) is $(+\frac{4}{7})$ and is a function of the number of links in the chain. This will be investigated for longer chains.

B. THERMOMECHANICS OF RUBBERLIKE ELASTICITY

In the preceding annual report, it was suggested that the correct statement of the combined expression for the first and second laws representing the thermomechanical deformation of a rubberlike material is given by:

$$dU = T\ell S + V^{+} \sum_{i} \frac{f_i \, d_T(\ell_i^{+} \lambda_i)}{\ell_i^{+} \ell_j^{+} \ell_k^{+}} \tag{71}$$

and not

$$dU = T\,dS + V^{+} \sum_{i} \frac{f_i \, d\,(\ell_i^{+} \lambda_i)}{\ell_i^{+} \ell_j^{+} \ell_k^{+}} \tag{72}$$

as is usually written. In (71) the differential is to be evaluated at constant temperature.

A simple argument shows that (72) does not predict the thermoelastic inversion. It may be rewritten as:

$$dU = T\,dS + V_o^{+} \sum \frac{f_i}{A^{+}_{io}} \, \frac{d\ell_i}{\ell^{+}_{io}} \tag{73}$$

Since the temperature change needed to define the slope of a force-temperature curve is only a few percent of the absolute temperature, it is an excellent assumption to replace the internal energy by:

$$U = U_o + C_\ell (T - T_o) \tag{74}$$

where the specific heat at constant length, C_ℓ, depends only on length but not on temperature. Using this, (73) becomes:

$$dS = \left(\frac{U_{oi} + C_{\ell i} (T - T_o)}{T} - \frac{V_o^+}{\ell_{io}^+ A_{io}^+} \frac{f_i}{T} \right) d\ell i + C_\ell \frac{dT}{T} \tag{75}$$

where the subscript "i" refers to partial differentiation with respect to ℓ_i. By Maxwell's relation, it develops that:

$$U_{oi} + C_{\ell i} (T - T_o) = \frac{V_o^+}{\ell_{io}^+ A_{io}^+} \left(f_i - T \frac{\partial f_i}{\partial T} \right) \tag{76}$$

which can be immediately integrated to yield:

$$f_i = \frac{T}{T_o} f_{io} - \frac{\ell_{io}^+ A_{io}^+}{V_o^+} \left[U_{oi} \left(\frac{T}{T_o} - 1 \right) - C_{\ell i} (T - T_o) + C_{\ell i} T \ell n \frac{T}{T_o} \right] \tag{77}$$

If we define the length dependences of the internal energy and specific heat in terms of the length dependence of the force, using two new parametera a and b, we can write:

$$\frac{\ell_{io}^+ U_{oi}}{V_o^+} = a \frac{f_{io}}{A_{io}^+} \tag{78}$$

$$\frac{\ell_{io}^+ C_{\ell i} T_o}{V_o^+} = b \frac{f_{io}}{A_{io}^+} \tag{79}$$

whereupon (71) becomes:

$$\frac{f_i}{A_{io}^+} = \frac{f_{io}}{A_{io}^+}\left[\frac{T}{T_o}(1-a+b) + (a-b) - b\frac{T}{T_o}\ell n\frac{T}{T_o}\right] \tag{80}$$

The force-temperature coefficient is then given by:

$$\frac{T_o}{A_{io}^+}\frac{\partial f_i}{\partial T} = \frac{f_{io}}{A_{io}^+}\left[1-a-b\,\ell n\frac{T}{T_o}\right] \tag{81}$$

Equation (81) clearly shows that a predicted thermoelastic inversion can only take place where f_{io} changes sign, that is, when the stress field goes from tensile to compressive, or vice versa, which is, in fact, not in agreement with observation.

Using the corrected version of the statement of thermomechanical deformation of a rubberlike material, one can arrive at a correct definition of the thermoelastic inversion, and a method for determining the parameters a and b . We have (71) in alternate form:

$$dU = T\,dS + V^+\sigma_i\,d\lambda_i = T\,dS + V^+ W_k\,dI_k \tag{82}$$

The Taylor's expansion of the internal energy is given by:

$$U = U_o + C_I\,(T-T_o) \tag{83}$$

where U_o and C_I depend only on $\{I_k\}$ (84)

Equation (82) becomes:

$$dS = \frac{U_{ok} + C_{Ik}\,(T-T_o)\,V^+W_k}{T}\,dIk + \frac{C_I\,dT}{T} \tag{85}$$

By Maxwell's relation, there develops:

$$\frac{U_{ok} + C_{Ik}(T-T_o)}{V^+} = W_k\,(1-3\alpha T) - TW_{kT} \tag{86}$$

which is readily integrated to:

$$W = W_o \frac{T}{T_o} \frac{V_o^+}{V^+} - \frac{(U_o - C_I T_o)(T-T_o)}{V^+ T_o} - \frac{C_I T \ell n (T/T_o)}{V^+} \tag{87}$$

The stretch dependences of the internal energy and specific heat are conveniently defined by setting:

$$\frac{U_o}{V_o^+} = a W_o \tag{88}$$

$$\frac{C_I T_o}{V_o^+} = b W_o \tag{89}$$

whereupon (87) becomes:

$$W = W_o \frac{V_o^+}{V^+} \left[\frac{T}{T_o} - (a-b) \left(\frac{T}{T_o} - 1 \right) - b \frac{T}{T_o} \ell n \frac{T}{T_o} \right] \tag{90}$$

The stress is given by:

$$\sigma_i = \frac{\partial W}{\partial \lambda_i} = W_{oi} \frac{V_o^+}{V^+} \left[\frac{T}{T_o} - (a-b) \left(\frac{T}{T_o} - 1 \right) - b \frac{T}{T_o} \ell n \frac{T}{T_o} \right] \tag{91}$$

The force is given by:

$$\frac{f_i}{A_{io}^+} = W_{oi} e^{-\int_{T_o} \partial dT} \left[\frac{T}{T_o} - (a-b) \left(\frac{T}{T_o} - 1 \right) - b \frac{T}{T_o} \ell n \frac{T}{T_o} \right] \tag{92}$$

The temperature coefficient of the force at constant length is given by:

$$\frac{T_o}{A_{io}^+} \frac{\partial f_i}{\partial T} \Big|_{\ell} = W_{oi} e^{-\int_{T_o} \partial dT} \left[1 - a - b \ell n \frac{T}{T_o} \right] - \alpha T_o \left[\frac{T}{T_o} - (a-b) \left(\frac{T}{T_o} - 1 \right) - b \frac{T}{T_o} \ell n \frac{T}{T_o} \right] e^{-\int_{T_o} \partial dT} \left[W_{oi} + W_{oik} \lambda_k \right] \tag{93}$$

Thus the exact condition for thermoelastic inversion is given by:

$$1 + \frac{W_{oik}\lambda_k}{W_{oi}}\Big|_{\text{th. inv.}} = \frac{1-a-b\ell n\,\frac{T}{T_o}}{\alpha T_o\left[\frac{T}{T_o} - (a-b)\left(\frac{T}{T_o}-1\right) - b\,\frac{T}{T_o}\,\ell n\,\frac{T}{T_o}\right]} \tag{94}$$

For the case of Neo-Hookean material, as an example, one has:

$$W_{oi} = \mu_o\left(\lambda_i - \frac{1}{\lambda_i^2}\right) \tag{95}$$

so that (94) becomes; in the limit $T \to T_o$:

$$\left(\frac{\ell_i}{\ell_{io}}\right)_{\text{th. inv.}} = \left(\frac{1-a+\alpha T_o}{1-a-2\alpha T_o}\right)^{\frac{1}{3}} \simeq 1 + \frac{\alpha T_o}{1-a} \tag{96}$$

or

$$\epsilon_{\text{th. inv.}} \simeq \frac{\alpha T_o}{1-a} \tag{97}$$

Conversely, the highly significant parameter a may be measured by the inverse of (97), or:

$$a = 1 - \frac{\alpha T_o}{\epsilon_{\text{th. inv.}}} \doteq 1 - \frac{.08}{.10} \tag{98}$$

where typical values for SBR have been inserted. Thus, it is expected that internal energy effects should account for ca. 20 % of the total stored strain energy, the other 80 % being stored as entropy. A fortiori, if all the energy is stored as entropy, a is zero, and the thermoelastic inversion strain exactly equals αT_o, for $\alpha T_o \ll 1$.

Now what (90) and/or (91) shows is that the temperature dependence of the strain energy is completely factorable from the stretch dependence. Thus, regardless of the magnitude of internal energy effects, there should be no effect upon the sign of the C_2 term, providing (88) and (89) are verified. This remains to be close experimentally.

For filled binders to which we are now in a position to turn our attention, it is expected that the value of $\underline{a}$ will be significantly higher than in the case of unfilled binders, for the simple reason that adhesion between binder and filler acts very much like interaction between chains. Furthermore, it has already been demonstrated that many filled binders dewet markedly, beyond which point the value of $\underline{a}$ should decrease markedly. These anticipated results will be documented in a later report.

In addition to evaluating $\underline{a}$ from the thermoelastic inversion, one can also procure it and $\underline{b}$ directly from the temperature dependence of $\sigma - \lambda$ data. What one does is to make Mooney-Rivlin plots at a series of temperatures, starting from T_o. The expected form of the relation representing the data should be very closely given by:

$$\sigma = \mu \left(\lambda - \frac{1}{\lambda^2}\right)\left(f_o + \frac{1-f_o}{\lambda}\right) \tag{99}$$

where

$$\mu = \mu_o \frac{V_o^+}{V^+}\left[\frac{T}{T_o} - (a-b)\left(\frac{T}{T_o} - 1\right) - b\,\frac{T}{T_o}\,\ell n\,\frac{T}{T_o}\right] \tag{100}$$

If one now introduces

$$\delta = \frac{T}{T_o} - 1 \tag{101}$$

then (100) becomes:

$$\frac{\mu}{\mu_o}\,\frac{V^+}{V_o^+} = 1 + (1-a)\,\delta - \frac{b}{2}\,\delta^2 \tag{102}$$

Thus a plot of

$$\left[\frac{(\mu/\mu_o)\,(V_o^+/V^+) - 1}{(T/T_o) - 1} \text{ vs } \left(\frac{T}{T_o} - 1\right)\right]$$

should yield a straight line with a negative slope $\underline{b/2}$ and an intercept $\underline{(1-a)}$.

Both a and b should be sensitive to filler content and plasticizer content and will be used to define adhesion properties in prospective propellant binders.

C. CREEP FAILURE OF GUM RUBBER VULCANIZATES

1. Introduction

Starting with a series of papers[2-9] by Bueche and later by Halpin[10, 11] there gradually developed a theory of the fracture of amorphous polymeric solids above the glass temperature. Inherent in this now widely accepted theory is the concept that the fracture process is a non-equilibrium one which includes the rupture of molecular bonds, the subsequent viscous flow of the newly separated polymer chains to relaxed configurations, the attendant growth of defects distributed throughout the solid, and the final fracture of the solid when the defects have grown to a critical number and size. Analysis of this concept leads to a relation between break time and break stress as well as between break time and break strain, for the assumed special case of simple tension, and which is shown on the basis of experimental data to be approximately insensitive to the test procedure used, that is, either to creep under constant load or to extension at constant rate of strain. In addition it is shown experimentally that data obtained at various temperatures can be correlated with the aid of a WLF shift factor.

Following a more phenological approach, Landel and Fedors[12] show that the break stress - break strain data can be correlated both in terms of a temperature shift factor and a crosslink-density shift factor.

In a completely formal approach, Coleman[13] uses extreme value theory and investigates the distribution of break times that develop as a result of iterated tests on a series of samples subjected to a given break procedure,

that is, to creep under a given load, or to extension at a constant rate, etc. Inherent in his theory is the concept of break time depending on sample dimensions as well as on break stress. There are no data presented however to show the importance of the sample dimension on the type of break time distribution that one might find empirically for a given class of amorphous polymeric solids.

As a result of the body of work accumulated in the literature on the basis of both formal and empirical approaches, it appears that there is a need for an elaborate empirical study of the break properties of a given amorphous polymer formulation. Such a study should include not only the empirical determination of the relation between break time and break stress under two types of loading processes, namely creep and constant rate of extension, but also the empirical determination of the distribution of break times at a given load or at a given rate of strain. This latter study has not been carried out by any of the previously cited investigators, despite the fact that it forms a critical test of the validity of any theory of fracture.

In addition, such a study should include the empirical determination of the break time-break stress relation and break time distribution function for several other stress fields besides that engendered in simple tension. This can be accomplished, for example, by means of observations on the creep to failure of thin solid disks (poker chips) bonded to two parallel loaded plates, and on the creep to failure of thin tubular cylinders (pipes) internally pressurized. Such tests have to date not been published in the open literature although the authors are aware of fragmentary pipe-burst data available in some industrial reports.

In addition, such a study should include the empirical determination of the effect of sample size upon the break time distribution function. This

effect will depend upon three time scales: the time required for molecular bond rupture, the time required for the newly separated chain ends to relax to an unstretched configuration, and the time required for a defect to grow into a crack large enough to provide for sample fracture. In the Bueche-Halpin theory, it is explicitly assumed that the second time scale is negligible with respect to the first. Because of this, no dependence upon sample dimension is predicted by their theory. This statement then provides a critical check of such data. And, it is proposed to present such data in a latter report of this series.

In addition, such a study should include the empirical determination of the temperature dependence of all parameters generated in the data correlation. Likewise, the way in which these parameters depend upon the chemical and physical structure of the rubber network should be investigated. Of particular importance would be the relation between mean break time and filler content and crosslink density. The latter can be modified either by varying the curative level or, as has been recently shown [14], by treating the network with a sulfur-removing agent, such as triphynyl phosphine. Such data will be presented in a later report of this series.

Finally, such a study should find a theoretical basis in a combined kinetic analysis of the initiation of defects, a stochastic analysis of the distribution of defects, and a dynamic mechanical analysis of the growth of defects and propagation of cracks. A kinetic analysis of the initiation of defects is the basis of the 1957 Bueche theory of fracture. In what follows we shall adopt a stochastic approach, assuming that defects are initially present and grow when stressed. In both the Bueche-Halpin theory, and the stochastic theory which we shall present, nothing is said about the

mechanics of defect growth or crack propagation. (This statement does not rule out the use of a stress concentration factor by Bueche and Halpin). It will be desirable therefore to supplement both theories by such a dynamic analysis as has been carried out by Knauss[15]. In the meantime, in the absence of such a dynamic theory of crack propagation, the present report will provide only a stochastic basis for the break time distribution. It will provide no basis for the break stress - break strain relation other than an empirical one, assuming that this is already fairly well treated by the Bueche-Halpin theory.

2. Stochastic Theory of Defects in Rubber Vulcanizates

A. Types of Defects Present in Rubber Vulcanizates.

There are two overlapping types of defects. One type includes pinholes which vary in size from 10μ (1μ = 10,000 $A^{o} \cong$ 4 blue light waves) down to 1,000 A^{o}. The upper range of such pinholes is visible under the microscope, the lower range just barely. The other type includes molecular-holes which vary in size from 1,000 A^{o} (a polymer chain of molecular weight 10^{6}) down to 10 A^{o} (a polymer chain of molecular weight 10^{2}, which would actually correspond to a short monomeric side chain). The upper range of such holes is visible under the electron microscope, the lower range just barely. Below this lower range, one gets into the realm of free volume perturbed by the thermodynamic vibration, rotation, and slow diffusion of polymer chain segments. Contrariwise, above the upper range of type one pinholes there exists the possibility of voids, or gas bubbles varying in size from 10μ upwards. Such voids are visible to the naked eye, are discerned in bulk by X-ray inspection, and can be ruled out of this discussion on the basis of good quality control. The pinholes of type one and

molecular holes of type two arise from irregularities in the mixing process, from poor dispersion of granular fillers like ZnO, and antioxidants, and from inhomogeneous diffusion of the polymer chains during cure in the hot press. Thus there results a vulcanizate in which the network is in general imperfectly cured, and is characterized by the presence and absence of dangling chain ends. The former leads to local variations in crosslink density, the latter to local variations in physical density, the latter to local variations in physical density. In addition there are somewhat grosser variations in density due to the dispersion of filler particles as aforementioned.

If one considers a cubic centimeter of SBR with a density of one gram per cubic centimeter, for a typical chain length of 10^4 between crosslinks, there are 10^{-4} moles of chains or 6×10^{19} chains. Each of these chains is about 80 A^o long and carries pendant side chains about 3 A^o long which number about ten percent of the total number of units in the backbone of the chain. If the primary molecular weight is 10^5, there are 10^{-5} moles of primary chains per cubic centimeter, each hooked by about ten crosslinks to other chains.

Now consider a sketch of a portion of a network for which the cross-linking functionality is f = 4.

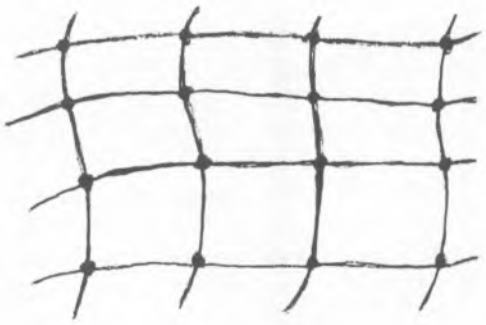

By direct count, the number of primary chains is given by N = 8, the number of crosslinked units is given by ν = 16. Since each crosslinked unit

generates f/2 chains (counted only once each), whereas each primary chain generates 2/2 chain ends (counted only once each), the total number of terminal end internal chains is given by:

$$N_t + N_i = 2\nu + N \doteq 40 \tag{103}$$

Similarly, the internal chains alone are given by:

$$N_i = 2\nu - N \doteq 24 \tag{104}$$

the terminal chains alone are given by:

$$N_t = 2N \doteq 16 \tag{105}$$

Thus the fraction of total chains which are dangling is given by:

$$f_d = \frac{2N}{2\nu + N} = \frac{2/M}{1/M_c} = \frac{2M_c}{M} \tag{106}$$

where $NM = (2\nu + N)\, M_c = N_o M_o = \rho \doteq 1 \text{ g/cc}$

and N is the number of primary chains/cc $\sim 10^{-5}$ moles/cc

M is the primary molecular weight $\sim 10^5$

ν is the number of crosslinked units/cc $\sim 4.5 \times 10^{-5}$ moles/cc

M_c is the chain molecular weight $\sim 10^4$

N_o is the total number of monomer units/cc $\sim 10^{-2}$ moles/cc

M_o is the monomer molecular weight ~ 100

For these rough ballpark numbers, it develops from (106) that about twenty percent of the chains form dangling ends; thus for a well-cured network, an important crosslink density fluctuation is to be expected throughout the network. This fluctuation will be important as far as failure properties go, but not as important in connection with small strain response.

In addition to defects of the types discussed above, another network characteristic will undoubtedly influence failure properties; this is the

presence of entanglements, loops, knots, and entwined network structures. As a result of these topological inhomogeneities, the local stress will be distributed as will the local strength. Thus the stress concentration around a strong defect point may be large enough to cause it to grow before another weak defect point around which there is a proportionately weaker stress concentration. Since very little can be said at the present time about the distribution of entanglements, and even less about the distribution of their strength properties, effects due to these irregularities shall be treated in a purely phenomenological manner.

B. Distribution of Defects in Undeformed Vulcanizate

1. Spatial Distribution of Defect Points.

Consider bulk polymer divided up into M cells labeled in some sequential order form 1, 2, ... to M. Consider further that there are N_1 defect points in cell 1, N_2 defect points in cell 2, etc., the total number of defect points being given by:

$$N = \sum_{s=1}^{M} N_s \tag{107}$$

What is the distribution function $\langle N_s \rangle$, i.e., what is the expected number of defect points in cell $\underline{s}$? Let p_s be the probability that a defect point occurs in cell $\underline{s}$. Then the probability of a given distribution $\{ N_s \}$ of defect points is given by:

$$\Omega = N! \prod_{s=1}^{M} \frac{p_s^{N_s}}{N_s!} \tag{108}$$

By the definition of probability, the sum of these overall probabilities (108) over all distributions must equal unity; i.e., -

$$Z \equiv \sum_{\Sigma N_s = N} N! \prod \frac{p_s^{N_s}}{N_s!} = 1 \tag{109}$$

By the multinomial theorem, (109) is equivalent to:

$$\sum_{\Sigma N_s = N} N! \prod \frac{p_s^{N_s}}{N_s!} = \left(\sum_{s=1}^{M} p_s \right)^N = 1^N = 1 \tag{110}$$

Thus the probability is normalized to unity.

Expressions for the moments of the distribution are now considered. By definition:

$$\langle N_r \rangle = \sum_{\Sigma N_s = N} N_r \Omega = \sum_{\Sigma N_s = N} N_r \, N! \prod \frac{p_s^{N_s}}{N_s!} \tag{111}$$

$$\langle N_r \rangle = N p_r \sum_{\Sigma N_s = N} (N-1)! \prod{}' \frac{p_s^{N_s}}{N_s!} \frac{p_r^{N_r - 1}}{(N_r - 1)!} \tag{112}$$

where the prime over the product symbol indicates that the r^{th} factor has been removed.

$$\langle N_r \rangle = N p_r \sum_{\Sigma N_s' = N-1} (N-1)! \prod \frac{p_s^{N_s'}}{N_s'!} = N p_r \, (\Sigma p_s)^{N-1} \tag{113}$$

where $N_s' = N_s$, for $s \neq r$, and $N_r' = N_r - 1$

$$\langle N_r \rangle = N p_r \tag{114}$$

Since,

$$\sum_{r=1}^{M} p_r = 1 \tag{115}$$

when all the $\{ p_r \}$ are equal, it follows that:

$$p_r = 1/M \tag{116}$$

so that

$$\langle N_r \rangle \Rightarrow \frac{N}{M} \tag{117}$$

which is simplest form of expectation based on a priori equal probability. This is the form one would expect for a completely homogeneous material.

The variance is given by:

$$\sigma_N^2 = \langle N_r^2 \rangle - \langle N_r \rangle^2 = \sum_{\Sigma N_s = N} N_r^2 \, \Omega - N^2 p_r^2 \tag{118}$$

$$\sigma_N^2 = \sum_{\Sigma N_s = N} N_r (N_r - 1) \, \Omega + N p_r - N^2 p_r^2 \tag{119}$$

$$\begin{aligned} \sigma_N^2 - N p_r + N^2 p_r^2 &= \sum_{\Sigma N_s = N} N! \prod{}' \frac{p_s^{N_s}}{N_s!} \frac{p_r^{N_r}}{(N_r - 2)!} \\ &= N(N-1) p_r^2 \times \sum_{\Sigma N_s = N} (N-2)! \prod{}' \frac{p_s^{N_s}}{N_s!} \frac{p_r^{N_r - 2}}{(N_r - 2)!} \end{aligned} \tag{120}$$

$$\sigma_N - Np_r + N^2 p_r^2 = N(N-1)p_r^2 \sum_{\Sigma N_s' = N-2}' (N-2)! \frac{p_s^{N_s'}}{N_s'!}$$

$$= N(N-1)p_r^2 (\Sigma p_s)^{N-2} \tag{121}$$

$$\sigma_N^2 = Np_r - Np_r^2 = Np_r(1-p_r) \Rightarrow N/M\ (1-1/M) \tag{122}$$

If M is large, we see that

$$\langle N_r \rangle \simeq \sigma_N^2 \approx N/M \tag{123}$$

Such a distribution, for which the mean equals the variance, is known as Poisson-type.

If an average cell is taken to be larger than several crosslinked units, then p_r will be small and fairly constant from cell to cell, in which case the distribution (114) will be well represented by (117); it will not be a packed distribution. On the other hand, if the average cell size is taken to be smaller than a crosslinked unit, then p_r will vary sharply from cell to cell depending upon the location of the dangling ends as well as on missing polymer fragments (voids, pinholes, free volume, etc.); in this case the distribution will be sporadically packed. Neither of these distributions are useful for stochastic analysis. Of more importance is the algebraic distribution of defects, which is now discussed.

2. Algebraic Distribution of Defect Points.

Also of interest is the expected number of cells that will contain s defect points. Let $\{M_s\}$ be the set of numbers of cells containing weak points, assuming a given distribution of such in the material. Then

$$\sum_{s=0}^{\infty} M_s = M \tag{124}$$

$$\sum_{s=0}^{\infty} sM_s = N \tag{125}$$

The overall probability of a given distribution of cell numbers (each of which contains s weak points) is given by:

$$\Omega = M! \prod_{s=0}^{\infty} \frac{(1/s!)^{M_s}}{M_s!} \tag{126}$$

In order to normalize this probability, one sums over all distributions to obtain:

$$Z \equiv \sum_{\substack{\Sigma M_s = M \\ \Sigma s M_s = N}} M! \prod_{s=0}^{\infty} \frac{(1/s!)^{M_s}}{M_s!} \tag{127}$$

$$Z = \text{coeff } z^N \text{in} \sum_{\Sigma M_s = M} M! \prod \frac{(z^s/s!)^{M_s}}{M_s!} = \text{coeff } z^N \text{in} \left(\sum_{0}^{\infty} z^s/s! \right)^M \tag{128}$$

$$Z = \text{coeff } z^N \text{in } e^{Mz} = \text{coeff } z^N \text{in} \sum_{k=0}^{\infty} \frac{M^k z^k}{k!} = \frac{M^N}{N!} \tag{129}$$

The expected number of cells is then given by:

$$\langle M_r \rangle = \frac{\Sigma M_r \Omega}{Z} = \frac{N!}{M^N} \sum_{\substack{\Sigma M_s = M \\ \Sigma_s M_s = N}} N_r M! \prod \frac{(1/s)^{M_s}}{M_s!} \tag{130}$$

$$\langle M_r \rangle = \frac{N!}{M^N} \text{ coeff } z^N \text{ in } \sum_{\Sigma M_s = M} M_r M! \prod{}' \frac{(z^s/s!)^{M_s}}{M_s!} \frac{(z^r/r!)^{M_r}}{M_r!} \tag{131}$$

$$\langle M_r \rangle = \frac{N!}{M^N} \text{ coeff } z^N \text{ in } \frac{Mz^r}{r!} \sum_{\Sigma M_s' = M-1} (M-1)! \prod \frac{(z^s/s!)^{M_s'}}{M_s'!} \tag{132}$$

$$\langle M_r \rangle = \frac{N!}{M^{N-1} r!} \text{ coeff } z^{N-r} \text{ in } \left(\sum z^s/s! \right)^{M-1} \tag{133}$$

$$\langle M_r \rangle = \frac{N!}{M^{N-1} r!} \text{ coeff } z^{N-r} \text{ in } e^{(M-1)z} = \frac{N!}{M^{N-1} r!} \frac{(M-1)^{N-r}}{(N-r)!} \tag{134}$$

or

$$\frac{\langle M_r \rangle}{M} = \binom{N}{r} \frac{(M-1)^{N-r}}{M^N} \tag{135}$$

For $r \ll N$, this simplifies to

$$\frac{\langle M_r \rangle}{M} = \frac{(N/M)^r e^{-M/N}}{r!} = \frac{m^r e^{-m}}{r!} \tag{136}$$

which is another form of Poisson-type distribution. From (136) it follows that the average number of defects per cell is given by:

$$\langle r \rangle = \sum_{r=0}^{\infty} r \frac{m^r e^{-m}}{r!} = m \tag{137}$$

Likewise the variance is given by:

$$\sigma_r^2 = \langle r^2 \rangle - \langle r \rangle^2 = \sum_{r=0}^{\infty} r^2 \frac{m^r e^{-m}}{r!} - m^2 = m \qquad (138)$$

Again it is noted that the variance equals the mean and that the distribution of numbers of cells with defect points depends only on the parameter m , which is the average number of defect points per cell. If one takes a cell to be 1 cc in size, and recall that there are about 10^{20} chains/cc , then it becomes quite probable that m is a large number. For example, if a defect point is located at every point where there is a dangling end, then m will be of the order of 10^{19} defects/cc.

C. Distribution of Defects in Deformed Vulcanizate

It is now assumed that, when the vulcanizate is maintained in stressed (deformed) state, some of the defects will become active and grow into cracks. One cannot forecast exactly when and where these cracks will appear, but can estimate the probability of their occurrence by considering the growth phenomenon to be a stochastic process.

Consider now one of the unit cells (say 1 cc in size), and assume that the cell contains a large number of defect points, as described above, each of which has the possibility to grow into a crack while the cell is maintained in a certain mechanical condition defined by a quantity φ, which depends only on the state of stress. To each defect point, there is also ascribed a critical value φ_g which is defined in such a way:

if $\varphi > \varphi_g$, the particular defect will grow to a crack and cause eventual rupture of the test specimen

if $\varphi < \varphi_g$, the particular defect will not grow.

Defects whose $\varphi_g < \varphi$ are termed active; defects whose $\varphi_g > \varphi$ are termed latent. If there are N_d defects in the unit cell, it is assumed that the distribution function of the φ_g is normalized by the relation:

$$N_d = \int_o^\infty f(\varphi_g)\, d\varphi_g \tag{139}$$

The question now arises: What is the expected number of active defect points in the unit cell? If p is the probability that any one defect point is active, then the probability that the cell contains x active defect points is given exactly by the binomial distribution:

$$p_x(x) = \binom{N_d}{x} p^x (1-p)^{N_d - x} \tag{140}$$

For $x \ll N_d$, this expression is well approximated by the Poisson distribution:

$$p_x(x) = \frac{(N_d p)^x \; e^{-N_d p}}{x!} \equiv \frac{m_d{}^x \; e^{-m_d}}{x!} \tag{141}$$

From (141), it follows that the expected number of active defect points is given by:

$$\langle x \rangle = \sum_{x=0}^{\infty} x P_x(x) = m_d = N_d p \tag{142}$$

On the other hand, from the definition of φ_g it follows that the expected number of active defect points is given by:

$$m_d = \int_o^{\varphi} f(\varphi_g)\, d\varphi_g \tag{143}$$

which is consistent with the statement that the probability of occurrence of an active defect point is given by:

$$p = \frac{1}{N_d} \int_o^{\varphi} f(\varphi_g)\, d\varphi_g \tag{144}$$

Since m_d depends on the state of stress through φ (as yet undefined), it is quite possible that m_d can be a large fraction of N_d, leading to a relatively high value of p. Just how many of the defects are activated depends on the relation between the mechanical state of stress and the failure criterion. It is now assumed that a state of constant true stress is applied which results in constant φ or m_d. The question then arises: What is the probability that one or more of these active defects becomes a crack?

D. Distribution of Cracks in Deformed Vulcanizate

In order to answer the preceding question, one needs to know the growth law. In lieu of speculating about the growth of defects, one can treat again the formation of a crack as a stochastic process by assuming there is another function $g(\varphi_g)$ which is the probability density per unit time for crack formation. Thus:

$$m_c = \int_o^{\varphi} g(\varphi_g)\, d\varphi_g \tag{145}$$

where m_c is the number of cracks which form per unit time. Nothing is known about $g(\varphi_g)$ except that it is Poisson-type and becomes more peaked (i.e., - approaches Gaussian type) as time elapses. Furthermore, $m_c t_b$ must be a small number, since macroscopic observations of failure show that once one or <u>two</u> cracks have formed, sample fracture occurs shortly thereafter.

Thus in order to calculate m_c, one can assume that

$$0 < \varphi_g < \varphi \ll \overline{\varphi}_g \equiv \frac{\int_0^\infty \varphi_g \, g(\varphi_g) \, d\varphi_g}{\int_0^\infty g(\varphi_g) \, d\varphi_g} \tag{146}$$

Over this range of integration, one then assumes that $g(\varphi_g)$ is continuous and monotonically increasing, and that

$$\left.\begin{aligned} &\frac{d\, g(\varphi_g)}{d\varphi_g} \Rightarrow 0 \\ \text{and} \quad &g(\varphi_g) \Rightarrow 0 \end{aligned}\right\} \quad \text{as } \varphi_g \Rightarrow 0 \tag{147}$$

These assumptions are equivalent to stating that the integration is carried out in the tail of a Gaussian distribution. Expanding $g(\varphi_g)$ in a Taylor's series, one obtains, in view of (147)

$$g(\varphi_g) = c_2 \varphi_g^{\,2} + c_3 \varphi_g^{\,3} \cdots \tag{148}$$

Neglecting terms beyond the quadratic, one obtains for (145)

$$m_c = \frac{c_2}{3} \varphi^3 = c \varphi^3 \tag{149}$$

where c is the crack rate proportionality constant which is assumed to be constant in time. This assumption is the weakest point in this theory. $\underline{\varphi}$ is a dimensionless function of the stress field.

Now, by an argument similar to that used in the preceding Section C, it can be shown that m_c is the expected number of cracks per unit time and that the actual crack probability distribution is given by:

$$Q(x) = \frac{e^{-m_c \Delta t} (m_c \Delta t)^x}{x!} \tag{150}$$

In writing (150) it is assumed that the stress field is uniform throughout the body from cell to cell (taken arbitrarily to be of 1 cc. size), so that φ is also uniform, and therefore also m_c by (149). The probability that there are no cracks formed in a time interval Δt is given by:

$$Q(o) = e^{-m_c \Delta t} \tag{151}$$

So, the probability that there develops one or more cracks per unit time between t and $t + \Delta t$ is given by:

$$\frac{1 - Q(o)}{\Delta t} = \frac{1 - e^{-m_c \Delta t}}{\Delta t} \tag{152}$$

Finally, the probability density per unit time that no cracks develop between time o and t_b and that one or more develop in the next increment Δt, is given by:

$$P(t_b) = \frac{e^{-m_c t_b} \left(1 - e^{-m_c \Delta t} \right)}{\Delta t} \tag{153}$$

Since one can shoose Δt to be arbitrarily small, (153) becomes in the limit

$$P(t_b) = m_c \, e^{-m_c t_b} \tag{154}$$

In the case of temporally non-constant but spatially uniform stress, (154) is readily generalized as follows:

First (149) becomes:

$$m_c(t) = c \, [\varphi \, (t)]^3 \tag{155}$$

Then

$$Q(o) = e^{-m_c(t) \Delta t} \tag{156}$$

$$P(t_b) = \frac{1 - e^{-m_c(t_b)\Delta t}}{\Delta t} \, e^{-\int_o^{t_b} m_c(t)\, dt} \tag{157}$$

$$P(t_b) = m_c(t_b) \, e^{-\int_o^{t_b} m_c(t)\, dt} \tag{158}$$

Equation (158) expresses the probability density per unit break time that a sample will rupture very shortly after the appearance of one or more cracks, whose rate of growth is expressed by (155) for a general time-dependent stress application.

One notes that (158) is normalized to unity, i. e. :

$$1 = \int_o^{\infty} P(t_b)\, dt_b = \int_o^{\infty} m_c(t_b) \, e^{-\int_o^{t_b} m_c(t) dt} \, dt_b \tag{159}$$

Let

$$\int_o^{t_b} m_c(t)\, dt \equiv u \tag{160}$$

so that (159) becomes

$$\int_o^{\infty} e^{-u}\, du = 1 \tag{161}$$

The expected break time is given by:

$$\langle t_b \rangle = \int_o^{\infty} t_b m_c(t_b) \, e^{-\int_o^{t_b} m_c(t)\, dt} \, dt_b \tag{162}$$

In the event that φ and therefore m_c is independent of time, it follows that:

$$\langle t_b \rangle \; m_c \text{ const.} = m_c \int_o^{\infty} t_b \, e^{-m_c t_b} \, dt_b = 1/m_c \tag{163}$$

Since, for a constant m_c , the observed break times evince considerable scatter, it is useful not only to know the mean or expected break-time, but

also the higher moments of the break-time distribution, i.e.:

$$\langle t_b^{\,n} \rangle_{m_c \text{ const.}} = m_c \int_o^\infty t_b^{\,n} \; e^{-m_c t_b} \, dt_b = n!/m_c \tag{164}$$

Thus the coefficient of variation is given by:

$$\frac{\sqrt{\langle t_b^{\,2} \rangle - \langle t_b \rangle^2}}{\langle t_b \rangle} = \frac{\sqrt{(2/m_c^{\,2}) - (1/m_c)^2}}{(1/m_c)} = 1 \tag{165}$$

which states that the standard deviation equals the mean value. For non-constant m_c, the mean break-time and its standard deviation must be calculated from a knowledge of how φ and therefore m_c depends on time. But φ depends on time implicitly through the stress field. Therefore it is necessary to introduce such a relation. We turn now to this point.

3. Relation Between Crack Rate and Stress Field

It has already been seen that, since $m_c t_b$ will be of the order of unity (Eqn. 163), a small number, it can be related to φ by integrating over the tail of a peaked Poisson distribution. This generated (149). The next question is: how does φ depend on the stress field? Based on data obtained on a polyurethane propellant[6], the suggestion is made that there is a critical stress level below which defects will not become active.

Just how φ depends on σ above this critical stress level is anybody's guess at the time of this writing. One simple proposal for uniaxial stress field may be:

$$\varphi = \begin{cases} 0, & \sigma < \sigma_{cr} \\ k\,(\sigma - \sigma_{cr})^n, & \sigma \geq \sigma_{cr} \end{cases} \tag{166}$$

For multiaxial stress field, one might have:

$$\varphi = \begin{cases} 0, & \dfrac{\sigma_1 - \sigma_2 + \sigma_3}{3} < \sigma_{cr} \\ k\,(\sigma_1 + \sigma_2 + \sigma_3 - 3\sigma_{cr})^n, & \dfrac{\sigma_1 + \sigma_2 + \sigma_3}{3} \geq \sigma_{cr} \end{cases} \tag{167}$$

or then again

$$\varphi = \begin{cases} 0, & \dfrac{\sigma_1 - \sigma_3}{2} < \sigma_{cr} \\ k\left[\dfrac{\sigma_1 - \sigma_3}{2} - \sigma_{cr}\right]^n, & \dfrac{\sigma_1 - \sigma_3}{2} \geq \sigma_{cr} \end{cases} \tag{168}$$

and so on. It is proposed to do a very careful study of break data on well characterized formulations in both uniaxial and biaxial stress fields and to search for a good phenomenological description of the relation between φ and σ_{ij} and then to compare this with the Bueche-Halpin theory. On the other hand, it is not believed that the study of the initiation and growth of single cracks in a viscoelastic medium subjected to large deformations is sufficiently far advanced at this time to enable one to deduce the equivalent of (166), (167) or (168) from first principles.

Following (166), it is noted that (163) becomes:

$$\langle t_b \rangle = \frac{1}{ck^3 (\sigma - \sigma_{cr})^{3n}}, \tag{169}$$

for $\sigma > \sigma_{cr}$ in simple tension

or

$$\ell n \langle t_b \rangle = - \ell n(ck^3) - 3n \ell n(\sigma - \sigma_{cr}) \tag{170}$$

Equation (170) has been applied to constant load creep data obtained by T. Smith[17] and J. Halpin[18]. In both cases the loads were converted to

true stress by multiplying by the measured stretch ratio at break. In Figure 2 is shown a plot of Smith's data, log breaking load vs log reduced breaking time, and also a plot of the converted log breaking stress vs. log breaking time. One notes that most of this plot is of the form of a straight line above the transition temperature, with a negative slope of (1/3). Furthermore when the true stress is corrected by subtracting off the critical true stress value of ca. 70 psi, all the data points in the rubbery region fall on a straight line. It is concluded that Eqn. (166) is an excellent representation for φ, with a value of n = 1.

The same procedure was applied to Halpin's data, Figure 3, except that the critical true stress was not determined. But again the usefulness of (166) is verified.

4. Distribution of Break Times

A. Theoretical

Consider now the scatter of the break times at a given stress level. Rather than computing moments of the distribution such as the mean break-time, the mean square of the break-time, etc., one can actually plot the cumulative fraction of samples that have break-time equal to or greater than some value T_b. This fraction, for constant m_c, is given by:

$$f = \int_{T_b}^{\infty} m_c \, e^{-m_c t_b} \, dt_b = e^{-m_c T_b} \tag{171}$$

This expression is to be contrasted with the one proposed by Coleman[19] based on extreme value theory, i.e.:

$$f = e^{-(T_b/A)^{1/B}} \tag{172}$$

The two expressions agree only in the event B = 1. Further, B is known to depend on sample size, whereas A or $1/m_c$ depends on the defect distribution, through $\langle t_b \rangle$. Thus, it is important to check the influence of sample size upon the scatter distribution as well as the effect of the load level (upon which $\langle t_b \rangle$ depends) upon the scatter distribution. In this report, the latter effect only is discussed.

B. Experimental

1. Preparation of Samples.

For the purpose of testing the theory of failure presented above, creep data under constant load were procured on a rubber formulation of the following composition:

Phillips SBR 1500 F	100 parts
Protox 166 ZnO	5.0 parts
Sulfur	1.5 parts
MBT	1.5 parts
Stearic acid	1.0 parts

After milling, batch sheets were molded on a hot press for one hour at 320°F. Ring specimens were cut from the sheets by a fly cutter. Such sheets display variable thickness from one region to another so that it was necessary to determine carefully the mean thickness of each ring as follows. A certain number of rings were weighed and also metered in all three dimensions on an optical comparator. It was found that the mean diameter was equal to 1.19" within .1 %, and the mean width equal to .0626" within 3 %. Thus the thickness could be sealed directly to the weight, and was found to be given by

$$t\ (\text{in}) = \frac{\text{ring weight (mg)}}{4140} = k\,W \qquad (173)$$

the overall mean thickness being .15" . Thus it was possible to accelerate the pace of sample preparation by merely weighing the ring prior to subjecting it to constant load, which load was in turn proportioned to the load necessary to provide a fixed engineering stress for rings of thickness 0.15 inch. In order to calculate the engineering stress, the following relation was used.

$$\sigma = \frac{L}{2t^+w^+} \tag{174}$$

where L is the load

w^+ is the width of the undeformed ring, and

t^+ is the thickness determined from the weight. If the thickness were different from 0.15 inch, the load was scaled accordingly to give a fixed stress.

To calculate the stretch ratio, the following relations[20] were used.

$$\lambda_i = 1 + \frac{2\Delta\ell}{\pi D_i^+} \tag{175}$$

$$D_i^+ = \langle D \rangle^+ - \frac{w^+}{2} \tag{176}$$

$$\lambda_a = \frac{\lambda_i + \dfrac{w^+}{D_i^+\sqrt{\lambda_i}}}{1 + \dfrac{w^+}{D_i^+}} \tag{177}$$

where $\Delta\ell$ is the increase in length of the ring, read by a linear variable differential transformer.

D_i^+ is the inside diameter of the unstretched ring.

$\langle D \rangle^+$ is the mean diameter of the unstretched ring.

λ_i and λ_a are respectively the inside and average stretch ratios. The average stretch ratio was used in reducing the data.

2. Data Reduction.

Rings were subjected to the following load levels: 0.90, 1.00, 1.10, 1.20, 1.30, 1.40, and 1.50 kg, always scaled to 0.15 inch thickness. At each of these load levels, 50 or more samples were allowed to creep to break at 75°F, and the break times and stretch-time curves were recorded. Figure 4 shows a plot of the observed break-times obtained at each of the applied loads. Table I summarizes some of the pertinent information obtained by averaging the break times and break stretch ratios at each load level. Column 1 gives the load in kg, Column 2 the engineering stress in kg/cm^2, Column 3 the mean break time in min., Column 4 the coefficient of variation of the break time, Column 5 the crack rate calculated from the first moment of the break-time distribution (Eqn. (163), Column 6 the crack rate calculated from the second moment of the break-time distribution (Eqn. 164), and Column 7 tabulates the mean stretch ratio at break. According to the theory developed (Eqn. 165) the coefficient of variation should be unity regardless of load. Figure 5 shows the excellent correlation with the theoretical slope of unity. The actual value averaged over the seven load levels is 1.246, and that averaged over all but the first load level is .827, which is probably as close as one can get to such a simple first-order theory after allowing for the intrinsic errors of sample measurement and testing. The unusually high value obtained for the data at 0.90 kg probably indicates a change in the mechanism of break associated with long break times of the

order of days. This inference probably reflects the effects of slow chemical degradation (oxidation and/or ozonation).

Again, barring the lowest load level, all crack rates calculated from first and second moments show exceedingly good agreement. This indicates that the data indeed do represent a theory of the type we have presented. To test this further, the distributions of break times for all load levels as suggested by the theory (Eqn. 171), were plotted in the form

$$-\ell nf = T_b/t_b \tag{178}$$

Figure 6 shows a plot of some of the data points obtained at all seven load levels. The theoretical line has, of course, a slope of unity, and the data thus evince excellent agreement with the theoretical equation (108). Note that the scatter increases as the load decreases, which bears out the previously stated inference that the mechanism tends to change as the break-time increases. One also notes that this correlation implies that the parameter B in the Coleman theory is unity. Since B is known to depend on sample size, we are in the process of repeating some of these experiments for larger rings.

In addition to testing ring specimens ab initio (i.e. - directly from the mold), other specimens were prestretched at 2"/min for ten cycles on the Instron to a stretch ratio of 400 percent. The same data were procured and reduced in like fashion; no significantly different results were found.

According to the relation (Eqn. 170) found for Bueche's and Halpin's data, the slope of a log-log plot of true stress vs. mean break time should have a negative slope equal to $1/3\,n$ where n is an empirical exponent in the expression (Eqn. 166) which relates the state of stress φ to the local stress field σ_{ij}. Such plots reduced from Smith's and Halpin's data

indicated a value of 1 for n. Contrariwise, a value of 2 (Figure 7) is found for the previously described formulation which is assumed to be quite similar to the Smith and Halpin formulations. In view of the large number of samples tested and the excellent fit of the data to the exponential distribution, as opposed to the relatively few samples tested by Halpin and Smith, it is concluded that the value 2 is a more meaningful number.

C. Conclusion.

After observing the excellent correlation presented in Figure 8, one concludes that the simple exponential function (178) is a very useful measure of the distribution of break times regardless of load. It remains to determine whether this correlation is independent of sample size. Furthermore it can readily be anticipated that since the fracture process is rate controlled by a viscoelastic mechanism, as pointed out by Halpin[11], that creep data obtained at various temperatures will be simply correlated on Figure 5 after multiplying $\langle t_b \rangle$ by a_T. Likewise data obtained in different stress fields and for vulcanizates of different cure types and cure densities should all follow the same correlation.

One expects however that the correlation shown in Figure 6 will show significant variation with temperature, stress field, chemical composition, and filler content. Just how the parameters k, n and σ_{cr} of Eqn. (169) as well as the forms of Eqns. (166 - 168) may depend upon stress cannot at this stage be anticipated although such questions do form legitimate basis for a dynamic mechanical investigation of defect growth and crack propagation.

D. TENSILE BEHAVIOR OF SWOLLEN AND UNSWOLLEN GUM RUBBER VULCANIZATES

1. Statistical Analysis of Ring Dimensions

The dimensions of a total of twenty rings, compounded according to the standard Kawabata formulation, were measured by means of the optical comparator. Figure 8 shows a plot of the mean area $\langle A \rangle$ of each ring (averaged over eight widths and six thickness measurements per ring) versus the weight, W, of the ring. The correlation is excellent, the correlation coefficient being 0.9880, and the regression line being given by:

$$\langle A \rangle^{(in^2)} = -0.0001752 + 0.01783\ W^{(g)}$$

with a standard error of .00022 sq. in. The white circles in Figures 8, 9, and 10 represent measurements on rings cut from the sheet referred to in the previous report. The black circles represent measurements made on rings cut from another sheet.

Figure 9 shows a similar correlation of mean thickness, $\langle t \rangle$, versus weight, W, the correlation coefficient being 0.9236, and the regression line being given by:

$$\langle t \rangle^{(in)} = 0.01918 + 0.1965\ W^{(g)}$$

with a standard error of .00644 inch.

Figure 10 shows the poor correlation which exists between mean width, $\langle w \rangle$, and weight, W, the correlation coefficient being .3736, which is not significant at the 95 % confidence level. The average ring has a mean width of 0.0787 in. with a coefficient of variation of 3.8 %. Alternatively if one averages the outside and inside diameter over the twenty rings, one finds the following results:

	Averaged over twenty rings, in.		Cutter dimension, in.
$\langle D_i \rangle$	1.1061	>	1.1055
$\langle D_o \rangle$	1.2638	>	1.2580
$\langle w \rangle = \frac{\langle D_o \rangle - \langle D_i \rangle}{2}$	.07885	>	.0763

Thus the mean width can be taken from measured average diameters, each of which is slightly greater than the cutter dimensions. This, and the poor mean width-weight correlation, indicate that the rubber is somewhat deformed and some material is lost during the cutting operation. An alternative method of cutting, in which the rubber sheet is held fixed by a metal plate, perforated with a hole of the right size, will be introduced. It is expected, on the basis of experience obtained with this method at Stanford Research Institute, that this technique will reduce the coefficient of variation of the width below one percent.

Summarizing: the new standard procedure will be to measure the dimensions of twenty rings for each sheet pressed from a mill batch. On each ring six measurements of thickness, eight of width, and four of internal diameter, will be taken. The mean thickness will be plotted versus weight and the regression line determined. The mean width will be obtained by straightforward averaging over all rings. This will then be taken as a fixed quantity for all rings of the same batch used in creep testing, while the thickness will be computed individually from the weight of each ring. For Mooney-Rivlin plots, it is only necessary to supply the additional information of mean inside diameter, which will also be taken as a fixed quantity for all rings of the same batch.

2. Effect of Solvents Upon the Mechanical Behavior of the Kawabata Formulation

Having made precise a method for determining the dimension of rubber rings, it is now possible to determine also precisely the initial stress under which a sample is allowed to creep, or the variable stress-strain relation evinced by tensile pull at constant elongation rate. We are now in the process of using the tensile pull at constant rate as a preliminary characterization of a series of batches of rubber rings, each batch having been treated with various reagents which affect both the sol fraction and chemical structure of the rubber. The motivation for this study is to determine the optimum chemical structure of possible binders. Subsequent to this preliminary characterization, additional creep tests will be run to assess the effect of the changes in sol fraction and chemical structure upon the creep failure characteristics which were described in MATSCIT PS 65-4, "A Research Program on Solid Propellant Physical Behavior," Quarterly Report No. 5 and 6, August 1965.

The sequence of tensile tests on samples treated with various reagents is projected as follows:

1. 6 raw samples pulled dry, 3 at +25°C, 3 at -24°C.
2. 6 samples swollen in toluene for two weeks, then vacuum dried for ten hours and pulled dry.
3. 6 samples swollen in toluene for two weeks, and pulled dripping wet (an immersion cup is being constructed).
4. 6 samples swollen in toluene, vacuum dried as above, and then refluxed with acetone for 16 hours, vacuum dried, and pulled dry.

5. 6 samples swollen in toluene, vacuum dried as above, and then refluxed with acetone for 16 hours, and pulled dripping wet.
6. 6 samples refluxed with acetone for 16 hours, vacuum dried as above, and pulled dry.
7. 6 samples refluxed with acetone for 16 hours, and pulled dripping wet.
8. 6 samples refluxed with acetone for 16 hours, vacuum dried, then refluxed for 16 days at 80°C with benzene solution made up to a composition based on two formula weights of triphenyl phosphine in solution per formula weight of sulfur in the rubber, then vacuum dried, and pulled dry.

The purpose of the toluene extraction is twofold: to leach out sol fraction and to determine the effect of cross-link density on the equilibrium swelling and on the second Mooney-Rivlin constant as measured by the tensile pull. The purpose of the acetone extraction is to leach out uncured or free sulfur and the purpose of the triphenylphosphine reaction is to change the cross-linking structure by removing sulfur as follows:

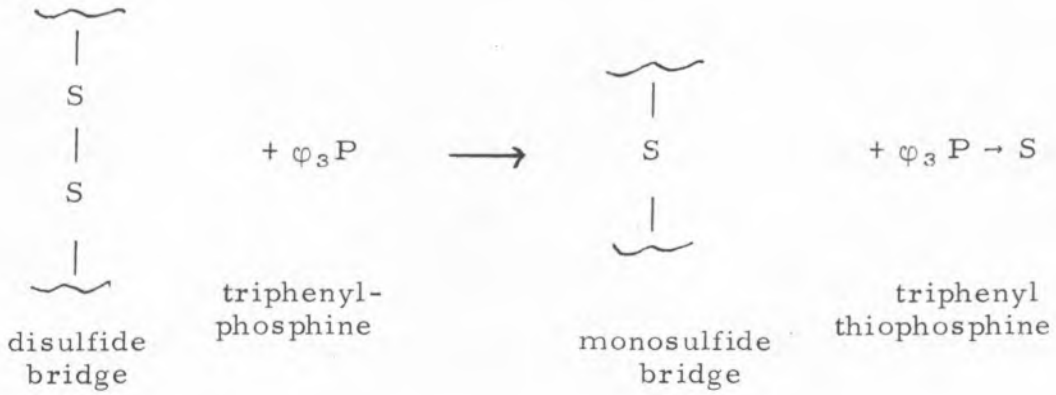

It is planned to carry this reaction out for various periods of time up to 16 days, after which time at least 95% of the cross-linked sulfur is removed

from bridges, the tetrasulfide bridges going sequentially to trisulfide to disulfide to monosulfide to zero sulfide. In addition, cyclic sulfur bridges doubly attached to the same chain are similarly reduced.

The Mooney-Rivlin plots for all the dry pulls - Cases 1, 2, 4 and 6 shown in Figures 11, 12, 13, and 14. In all four cases the data obtained at both temperatures evince a form characteristic of Mooney-Rivlinear materials, the data at the lower temperature showing an additional upturned segment characteristic of a network of finite length chains. The straight-line parameters of the eight curves are summarized in Table II.

It appears that the only significant difference which stands out in Table II is the increase in f at ambient temperature from .10 to .20 as a result of treatment with solvents. Not quite as striking is the increase in shear modulus. Both of these increases are consistent with a removal of sol fraction which increases cross-link density. In the next report we shall show the effects of swelling upon the slope (1-f) of the Mooney-Rivlin plots. Beyond that, it is anticipated that greater effects will show up in the records of the creep data which will be obtained during the next six months.

3. Swelling of Rings in Toluene

Prior to pulling the rings dripping wet (cases 3, 5, 7, Table II), it is necessary to record the wet dimension, and to observe how rapidly the rings swell timewise in order to determine a practical upper limit to swell duration. For this purpose a traveling microscope has been constructed in the Polymer Science Laboratory. A correlation between weight and thickness will be obtained on this apparatus for another twenty rings. The first five results are shown in Figure 15. If it develops that the standard error incurred with this apparatus does not exceed ten percent, it will be used in

place of the more time-consuming and less convenient measurements on the optical comparator.

4. Solvent Treatment of the Kawabata Formulation

A sequence of solvent treatments has been applied to the Kawabata formulation to study the effect of removal of sol fraction and the effect of swelling upon the Mooney-Rivlin plot, these treatments all being prior to the determination of creep failure data. The Mooney-Rivlin plots for the wet samples are shown in Figures 16, 17 and 18, where there are recorded tensile pulls at 1"/min (three samples at +24°C, three at -24°C) for samples:

a) swollen in toluene for two weeks, and pulled dripping wet.

b) swollen in toluene, vacuum dried, refluxed with acetone for 18 hours, and pulled dripping wet.

c) refluxed with acetone for 18 hours, and pulled dripping wet.

In contrast to the four plots shown above for the tensile pulls on dry samples, Figures 16, 17 and 18, evince nearly straight-line behavior with a slope close to zero in all cases. Thus, both toluene and acetone are effective in reducing entanglements between chains, and concatenately in reducing C_2 to zero, or increasing f to unity. These conclusions are summarized in Figures 19 and 20 from which it also becomes clear that the shear modulus is reduced markedly as a function of swelling. Finally, one notes that acetone is not quite as efficient a swelling agent as toluene, although pretreatment with toluene seems to render the acetone somewhat more effective.

In order to expedite the swelling process, the change in dimension of a ring was metered with the traveling microscope over a period of two weeks.

It is apparent from Figure 21 that most of the swelling is completed within 12 hours. Thus, for future testing purposes, it will not be necessary to swell for more than one day.

Likewise, it will be prudent to expedite the acetone extraction by determing how long it takes to remove free sulfur. An analytical technique for doing this is now being checked out.

5. Optimization Studies on SBR-MBT and SBR-MBTS Formulations

As a result of previous studies, it was determined that a so-called optimum formulation in terms of maximum elongation was achieved by plasticizing the Kawabata formulation with 20 parts DOP. For such plasticized formulations a further study was made to determine optimum S-MBT or optimum S-MBTS concentration and optimum cure time and temperature. The results are shown in Figures 22, 23, 24 and 25, for tensile pulls at $+24^{\circ}C$ and $-30^{\circ}C$.

It is apparent particularly from the $+24^{\circ}C$ data that formulations below 0.6 S-MBT or 0.6 S-MBTS tend to become tacky. Also, there is no significant difference between MBT and MBTS although there may be some effect as regards oxidative stability with time. This remains to be determined. Furthermore, there is little or no significant difference among the various cure histories. From now on it is decided to cure for one-half hour at $325^{\circ}F$. This completes the optimization study. The particular formulation based on 0.6 S-MBT or 0.6 S-MBTS will be used for creep failure studies along with the Kawabata formulation in uniaxial, biaxial, and triaxial stress fields.

E. CHEMICAL ANALYSIS OF SULFUR IN MILLED MASTER BATCHES AND GUM VULCANIZATE

1. Introduction

In order to provide quality control over crosslink density, it is necessary to develop analytical techniques for the determination of free sulfur and crosslinked sulfur prior to the correlation of crosslink density with physical properties. At present three problems are being worked on:

a) determination of the change with time of the concentrations of free sulfur and crosslinked sulfur in cured and uncured (master batches and mill batches) rubber.

b) determination of the change in concentrations of free sulfur and crosslinked sulfur after extraction with acetone.

c) effect of selective attack of polysulfide linkages by triphenylphosphine.

Three methods are being used to determine sulfur in the rubber samples:

a) Determination of total sulfur as $BaSO_4$.

The rubber is digested in f. HNO_3 and Br_2. After treatment the $SO_4^=$ is precipitated as $BaSO_4$ and determined gravimetrically.

b) Determination of free sulfur as thiosulfate.

The rubber is digested in Na_2SO_3 and the thiosulfate formed is titrated isdometrically.

c) Determination of all sulfur simultaneously.

i) Free sulfur is determined as H_2S liberated from rubber samples refluxed in HCl - ether solution.

ii) Polysulfide sulfur is determined as $S^=$ titrated potentiometrically.

iii) Mono- and di-sulfide linkages are determined as the mercaptan titrated potentiometrically (in the same titration as above).

2. Analytical Results

Progress that has been made toward the goals mentioned above include:

a) Determination of the free sulfur content of the sulfur-containing Master Batch (MB 2).

Total sulfur in MB 2 = 23.08 ± .05%, prepared 1 March 1965.

Free sulfur in MB 2 = 17.78 ± .22%, determined 1 December 1965.

The free sulfur was determined by method b) above.

b) Samples of Mill Batches 1 and 2 with MBTS and Mill Batch 1 with MBT have been prepared for titration. The free sulfur will be determined by method b).

II. PHYSICOMECHANICAL BEHAVIOR OF FILLED GUM RUBBER VULCANIZATES

A. INTRODUCTION

At this point in the program of study on the physicomechanical behavior of rubber vulcanizates, the groundwork has been laid for the determination of failure properties. A stochastic method has been developed for correlating break time and break stress in increased tension. The method will be applied to samples subjected to bi- and tri-axial tension at various temperatures. The failure surfaces will be plotted and correlated with crosslink density. Internal energy effects will also be evaluated.

This same procedure will now be applied to filled binders. As a start in this direction, we have elected to introduce a new concept in binder type. As is well known, a filled rubber gets its strength both from crosslinks and from adhesion. However, the crosslink density can not be too high or ultimate elongation becomes too low. In order to avoid this problem, one can omit chemical crosslinks entirely, while providing good adhesion as well as physical crosslinks. An excellent candidate for this type of binder is the thermoplastic rubber Kraton (Shell Development Company) based on styrene-butadiene-styrene triblock polymers. At ambient temperature the styrene is below its glass transition temperature, and thus acts as a crosslink whether or not filler is dissolved in the glass phase. The butadiene, on the other hand provides high elongation and high adhesion to filler. The major difficulty with such a system is susceptibility to air oxidation. An alternate candidate chosen from the Kraton series is based on styrene-isoprene-styrene which is much more stable toward oxidation. Both of these candidates are being used to prepare glass bead-filled resins with 50 vol. % beads of 30μ diameter. Tensile data are being procured.

REFERENCES

1. Edwards, S. F.: The Statistical Mechanics of Polymers with Excluded Volume. Proc. Phys. Soc. 85, 613, (1965).

2. Bueche, F.: Journal of Chemical Physics, 25, 603 (1954).

3. Bueche, F.: Journal of Chemical Physics, 26, 738 (1955).

4. Bueche, F.: Journal of Polymer Science, 24, 189 (1957).

5. Bueche, F.: Journal of Applied Physics, 26, 1133 (1955).

6. Bueche, F.: Journal of Applied Physics, 28, 784 (1957).

7. Bueche, F.: Journal of Applied Physics, 29, 1231 (1958).

8. Bueche, F.: Rubber Chemistry and Technology, 32, 1269 (1959).

9. Bueche, F.: Journal of Applied Polymer Science, 7, 1165 (1963).

10. Bueche, F., and Halpin, J. C.: Journal of Applied Physics, 35, 36 (1964).

11. Halpin, J. C.: Journal of Applied Physics, 35, 3133 (1964).

12. Landel, R. F., and Fedors, R. F.: Chapter III B of Fracture Processes in Polymeric Solids, edited by B. Rosen (1964).

13. Coleman, B.: Journal of Applied Physics, 29, 968 (1958).

14. Moore, C. G., and Trego, B. R.: Journal of Applied Polymer Science V, 299 (1961).

15. Knauss, W. G.: Rupture Phenomena in Viscoelastic Materials, Ph.D. Dissertation, California Institute of Technology, June 1963.

16. Blatz, P. J.: Eighteenth Meeting Bulletin of JANAF Panel on Physical Properties of Solid Propellants, 17, June 1959.

17. Smith, T. L.: Journal of Polymer Science, A 1 , 3597 (1963).

18. Halpin, J. C.: Journal of Applied Physics, 35, 3133 (1964).

19. Coleman, B.: Journal of Applied Physics, 29, 968 (1958).

20. Blatz, P. J.; George, N.; and Kawabata, S.: "Physicomechanical Behavior of Rubberlike Materials," AFRPL-TR-65-112, Edwards Air Force Base, California, April 1965. MATSCIT PS 65-2, California Institute of Technology, April 1965.

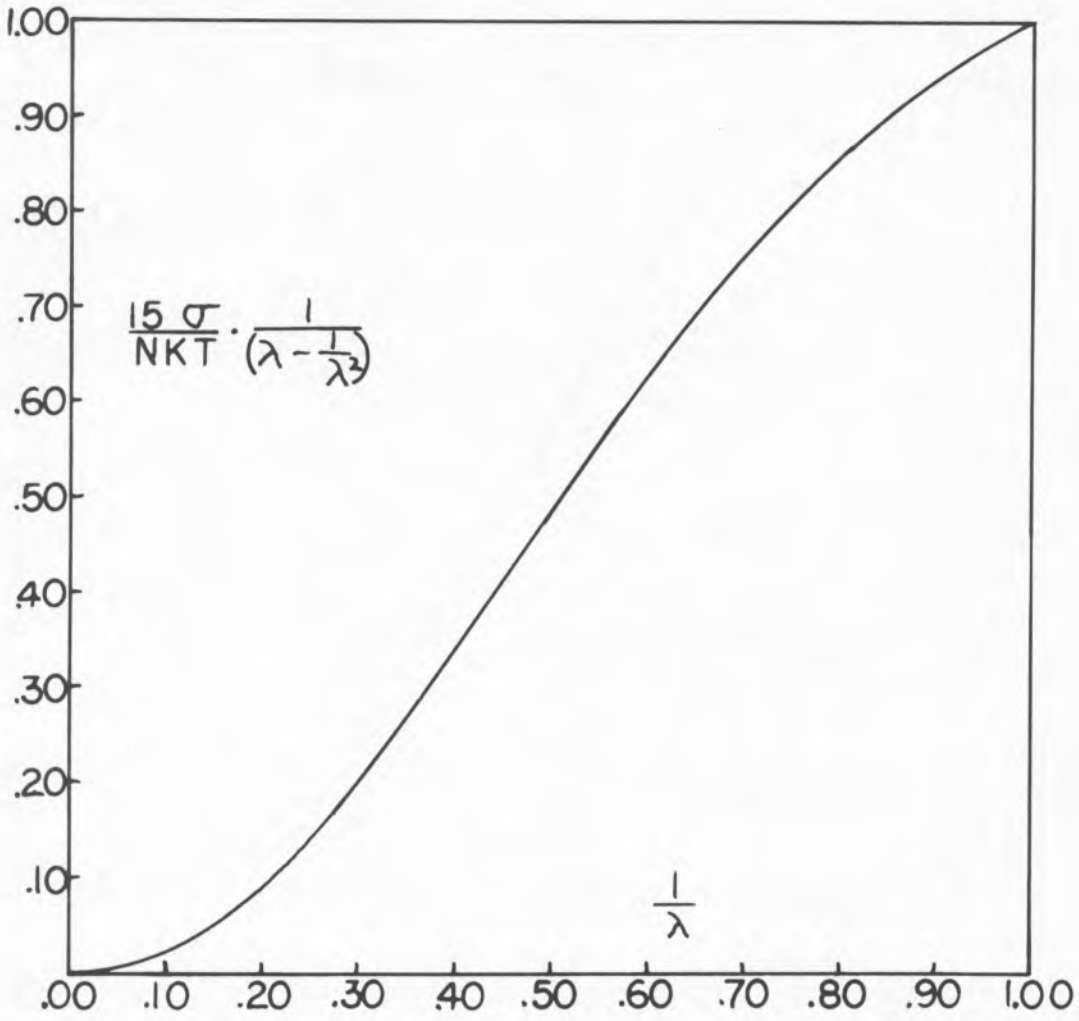

Figure 1. Mooney-Rivlin Plot for Non-Affine Deformation of 2-Link Chain.

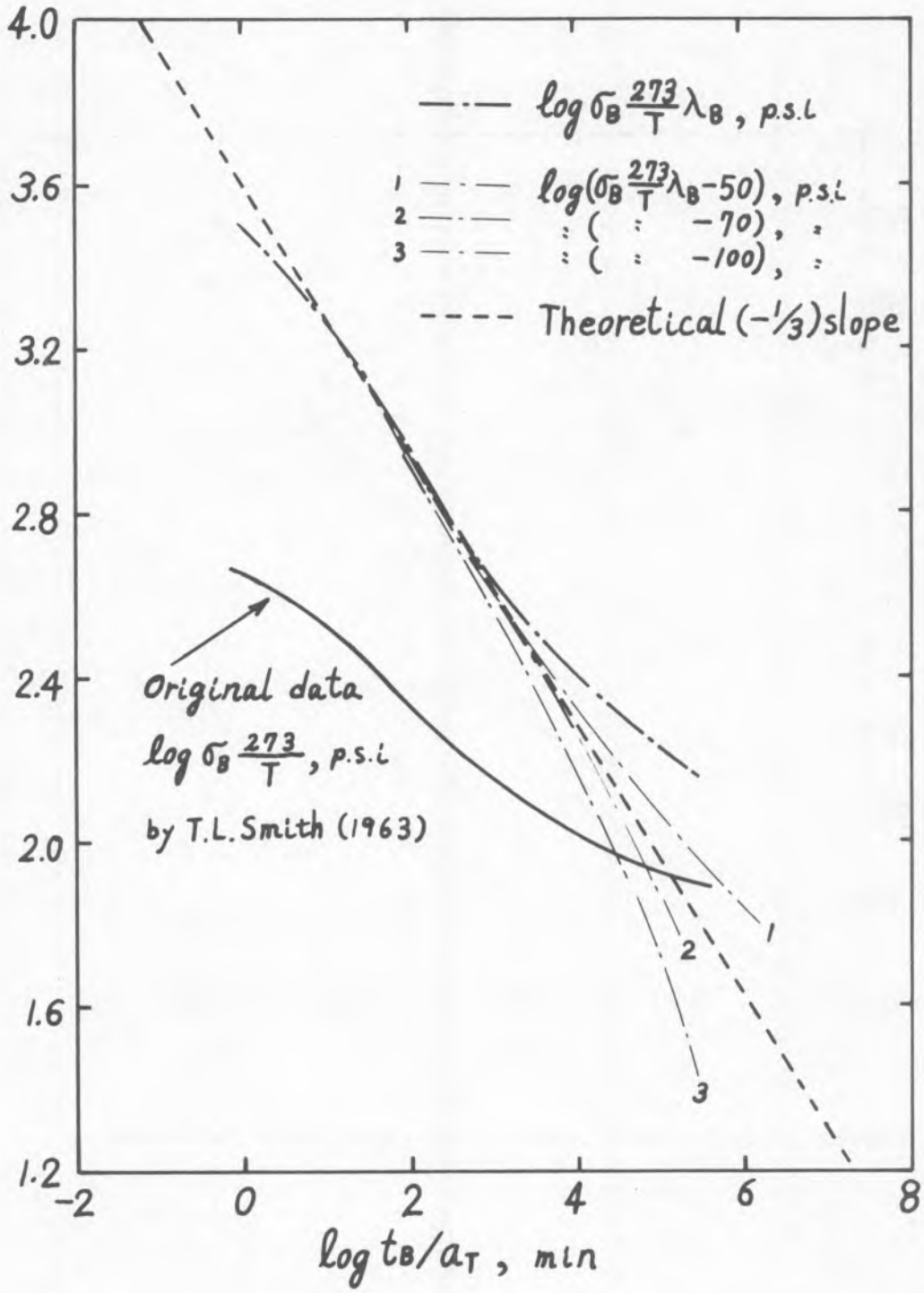

Figure 2. Break Stress-Break Time Data Determined by T. Smith.

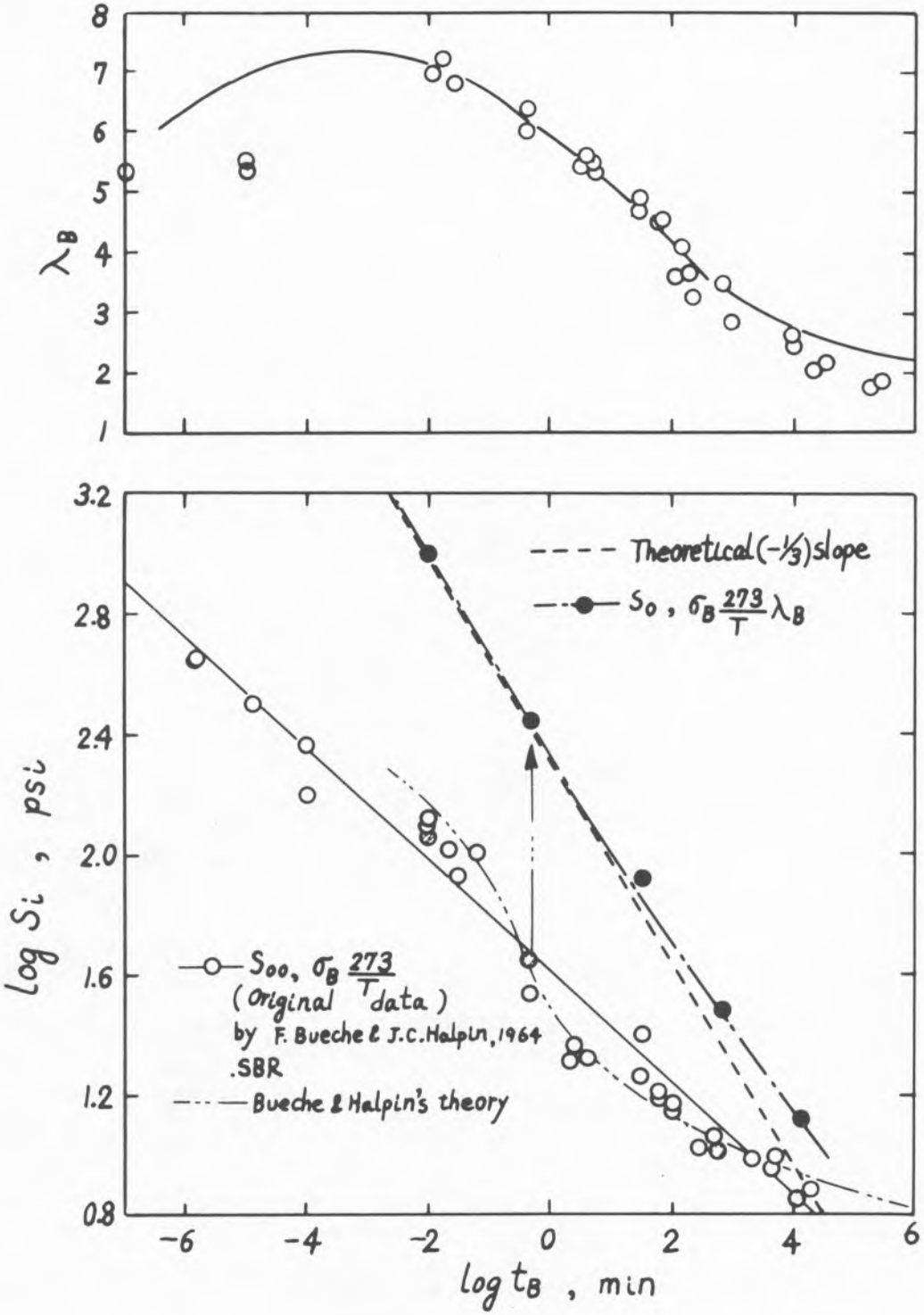

Figure 3. Break Stress-Break Time Data Determined by J. Halpin.

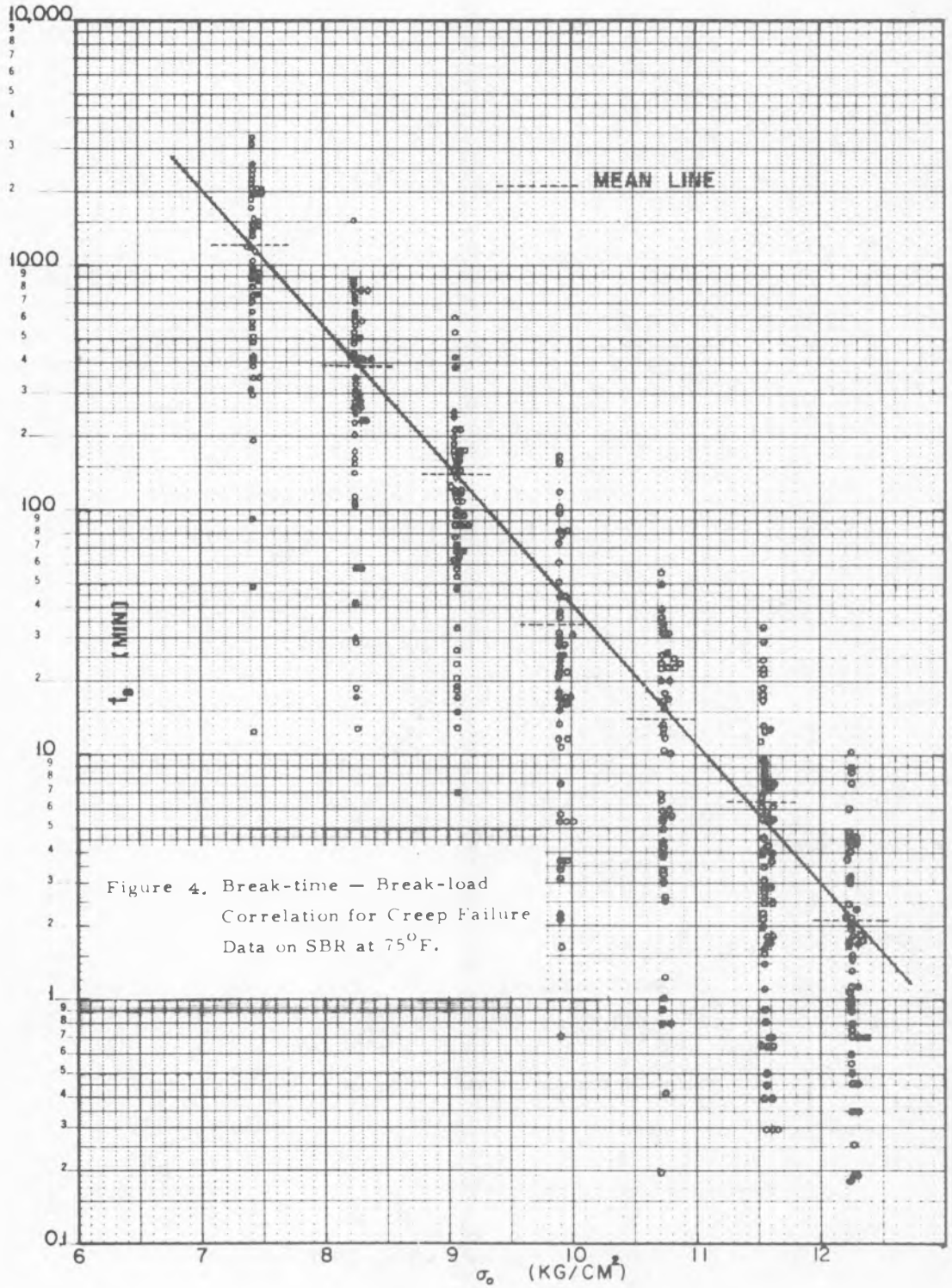

Figure 4. Break-time — Break-load Correlation for Creep Failure Data on SBR at 75°F.

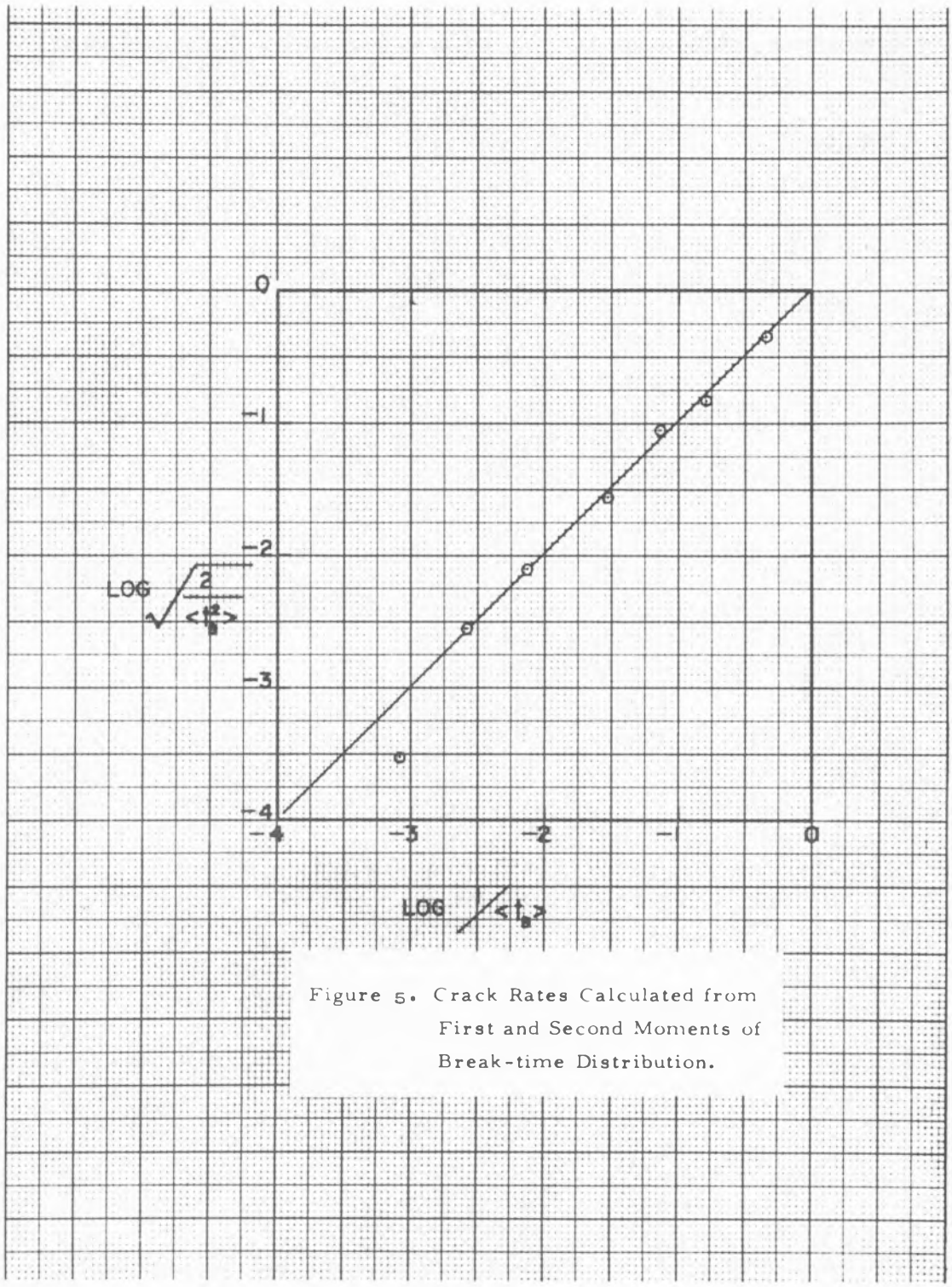

Figure 5. Crack Rates Calculated from First and Second Moments of Break-time Distribution.

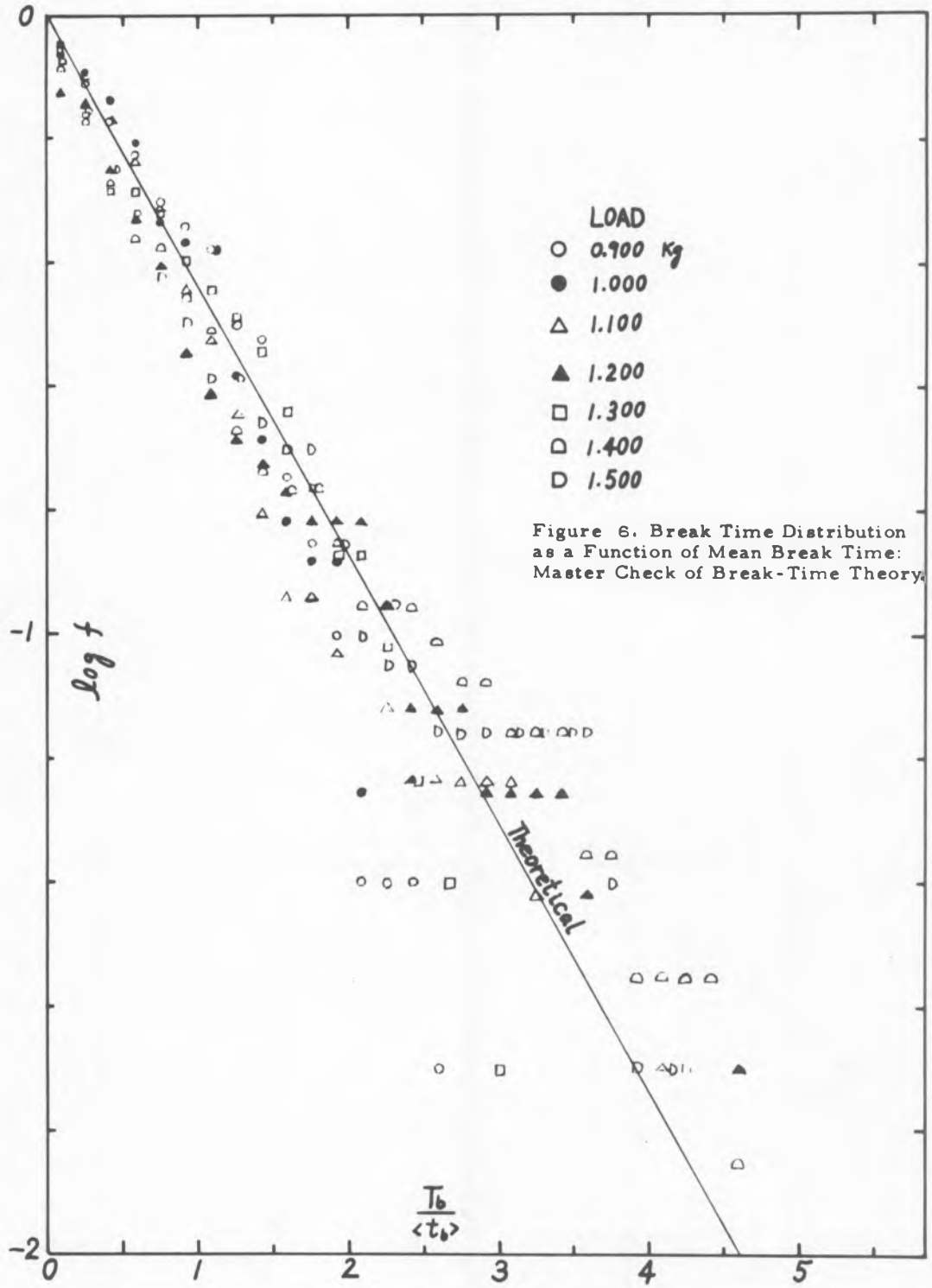

Figure 6. Break Time Distribution as a Function of Mean Break Time: Master Check of Break-Time Theory.

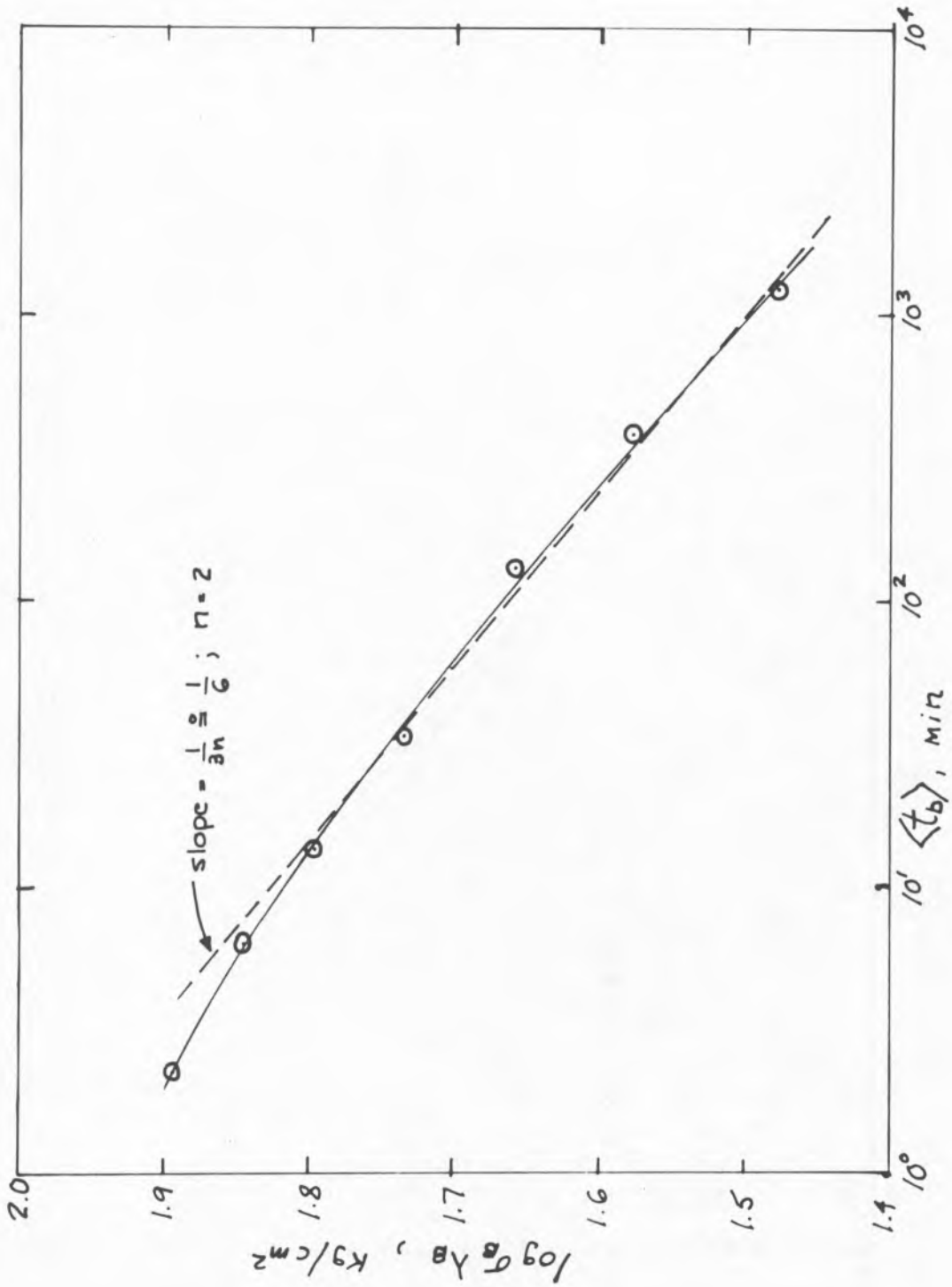

Figure 7. Correlation Between Mean Break Time in Creep and True Stress Level in Simple Tension.

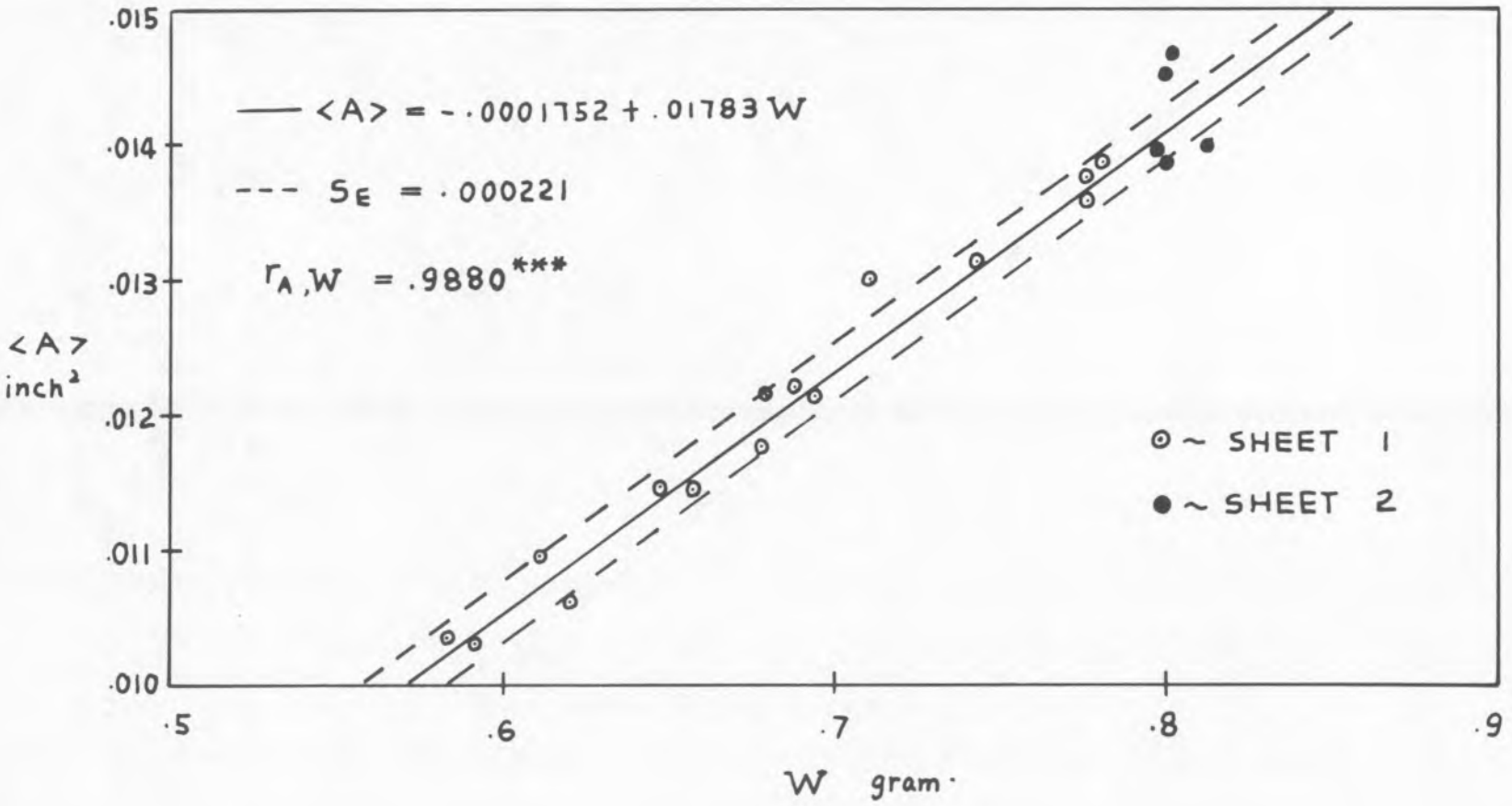

Fig. 8. AREA – WEIGHT CORRELATION

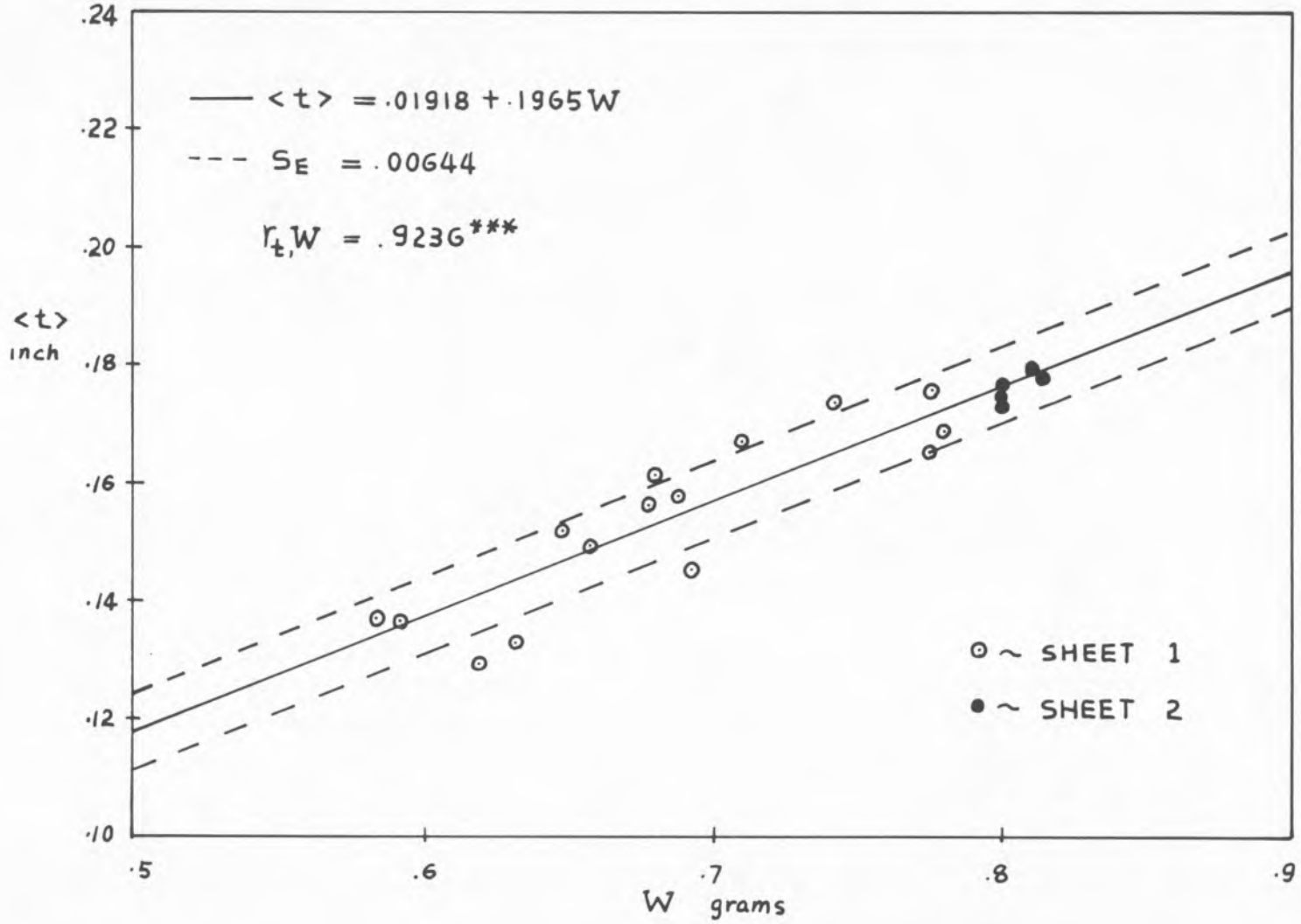

Fig. 9. THICKNESS – WEIGHT CORRELATION

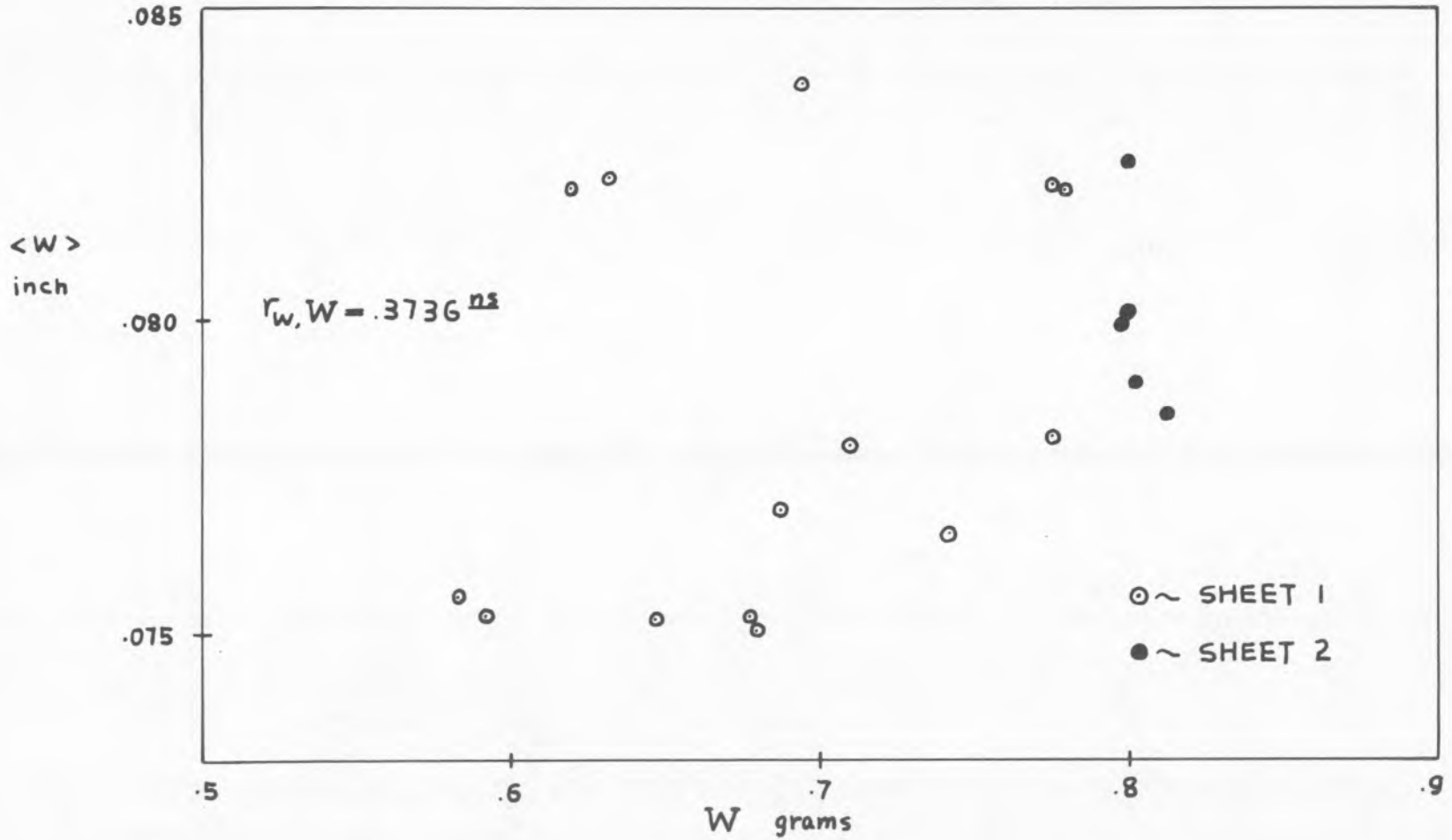

Fig. 10. WIDTH-WEIGHT CORRELATION

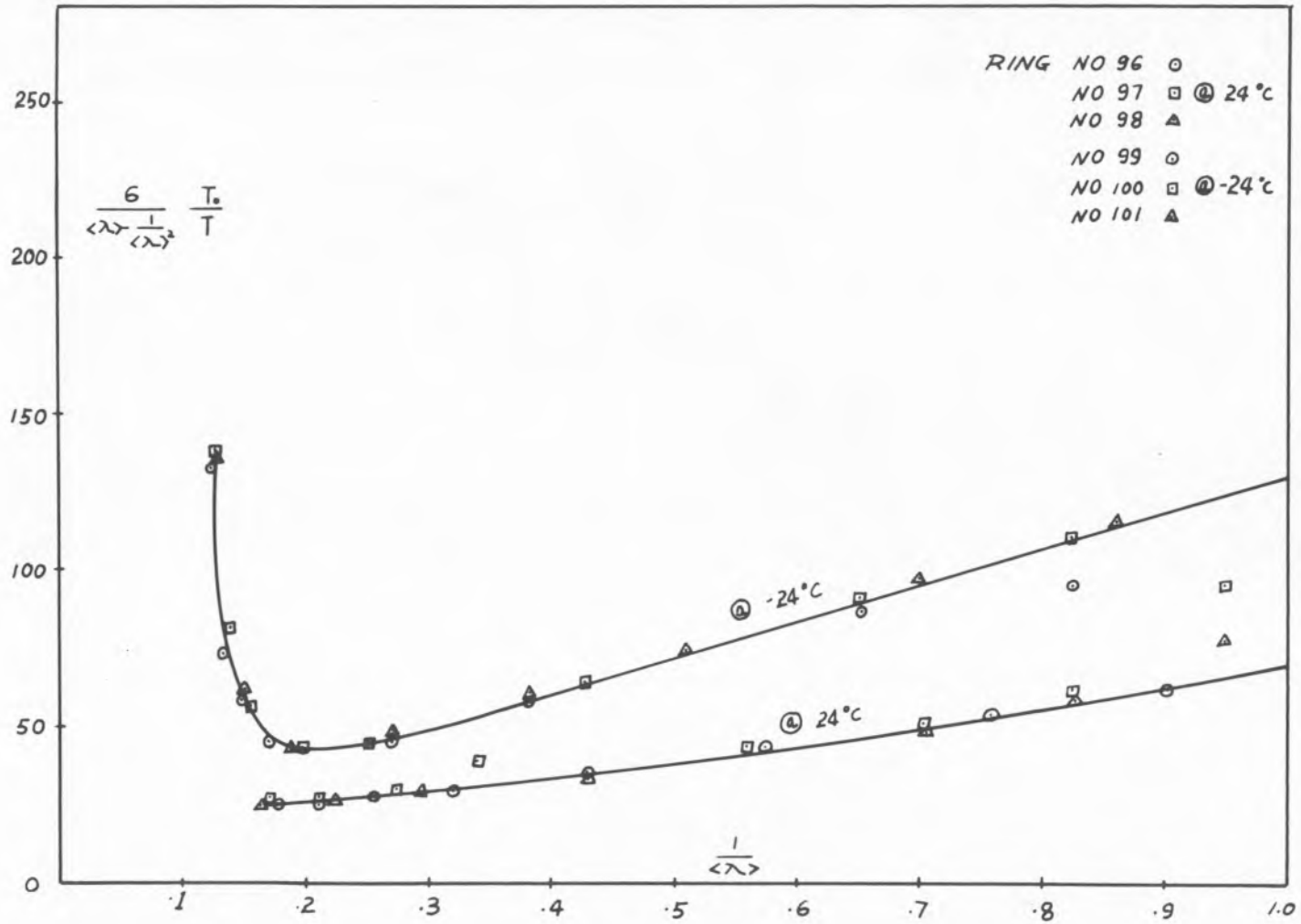

Fig. 11. SBR-MBT-S UNSWOLLEN

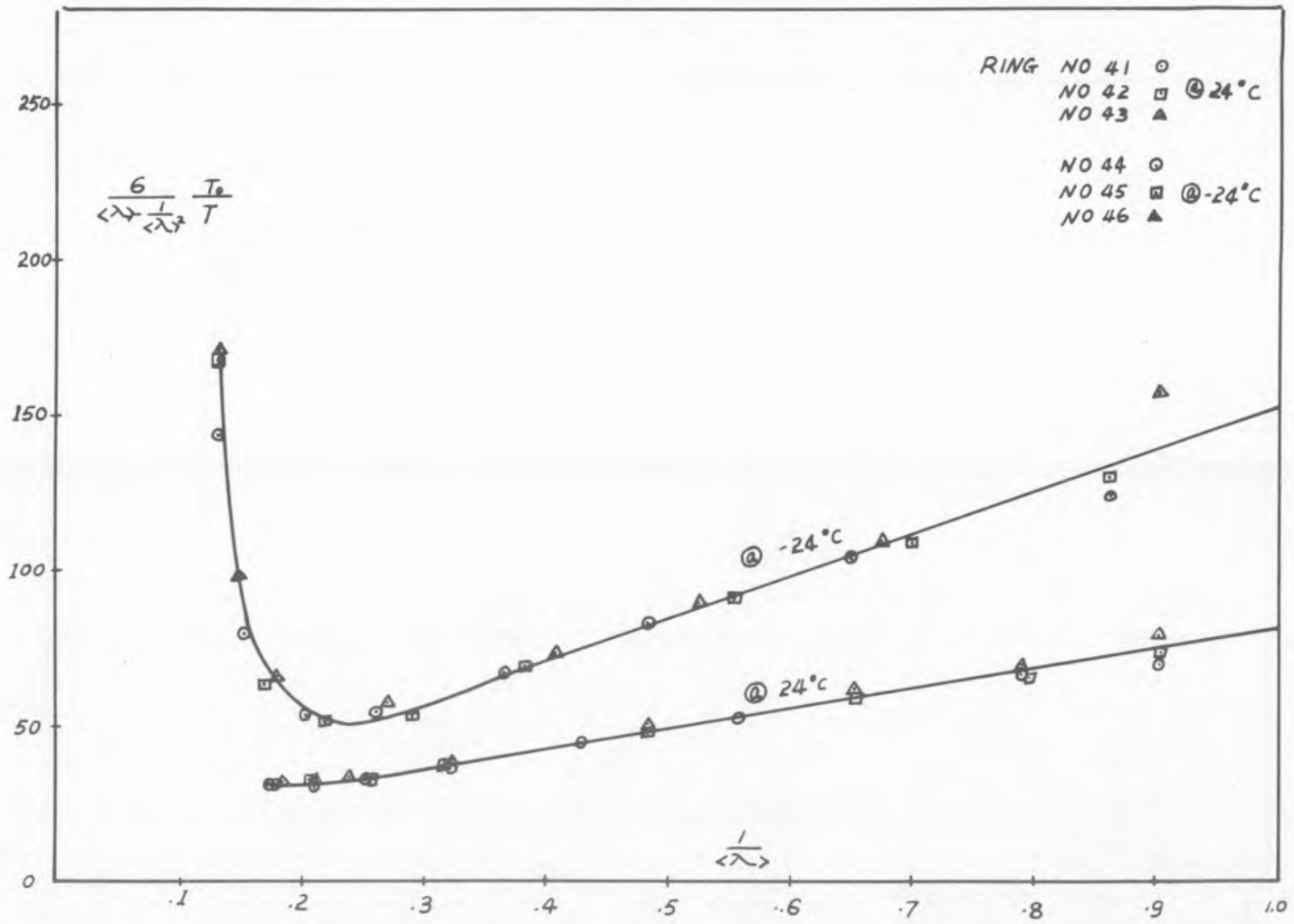

Fig. 12. SBR-MBT-S SWOLLEN IN TOLUENE, VACUUM DRIED

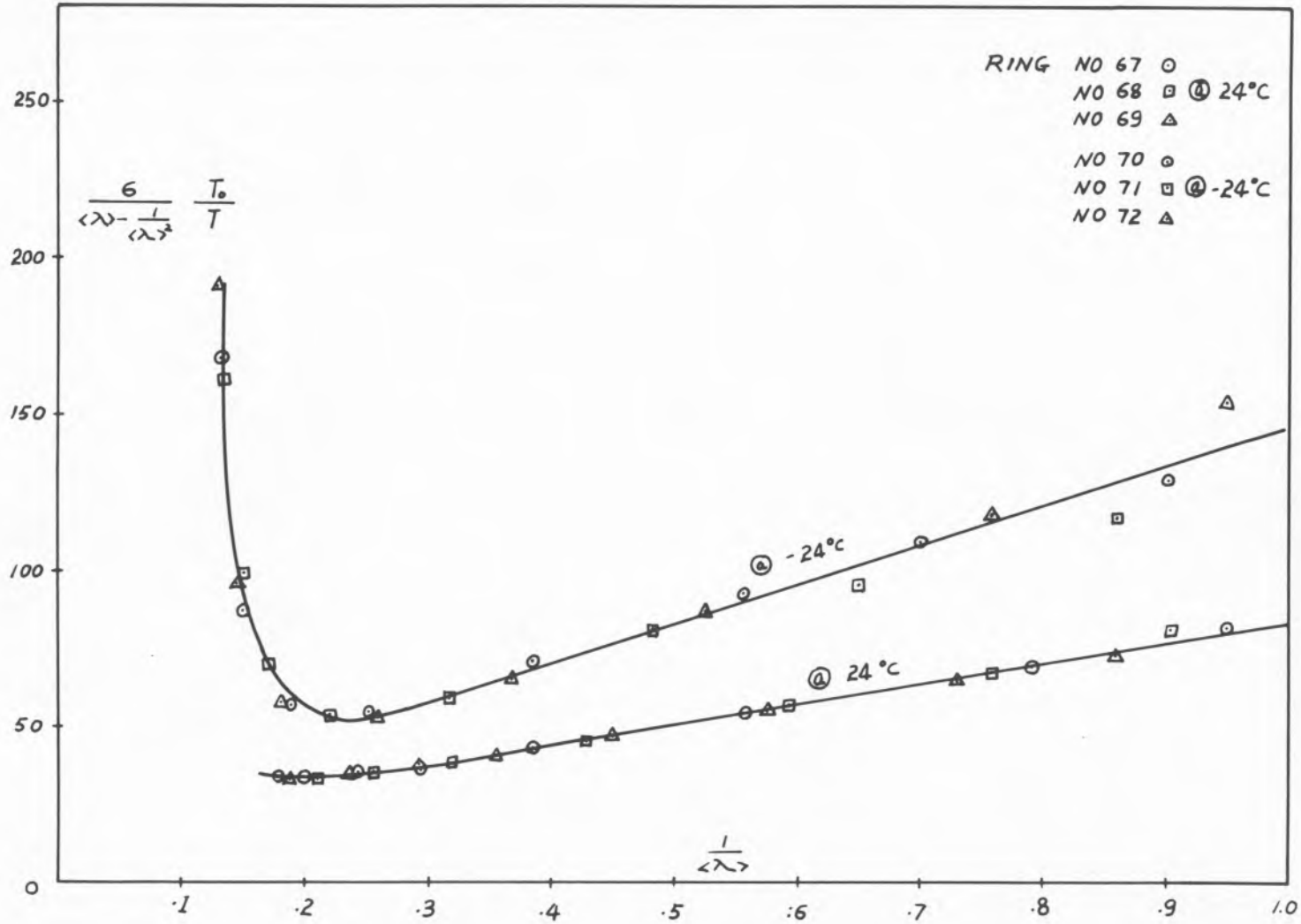

Fig. 13. SBR-MBT-S SWOLLEN IN TOLUENE, ACETONE EXTRACTED

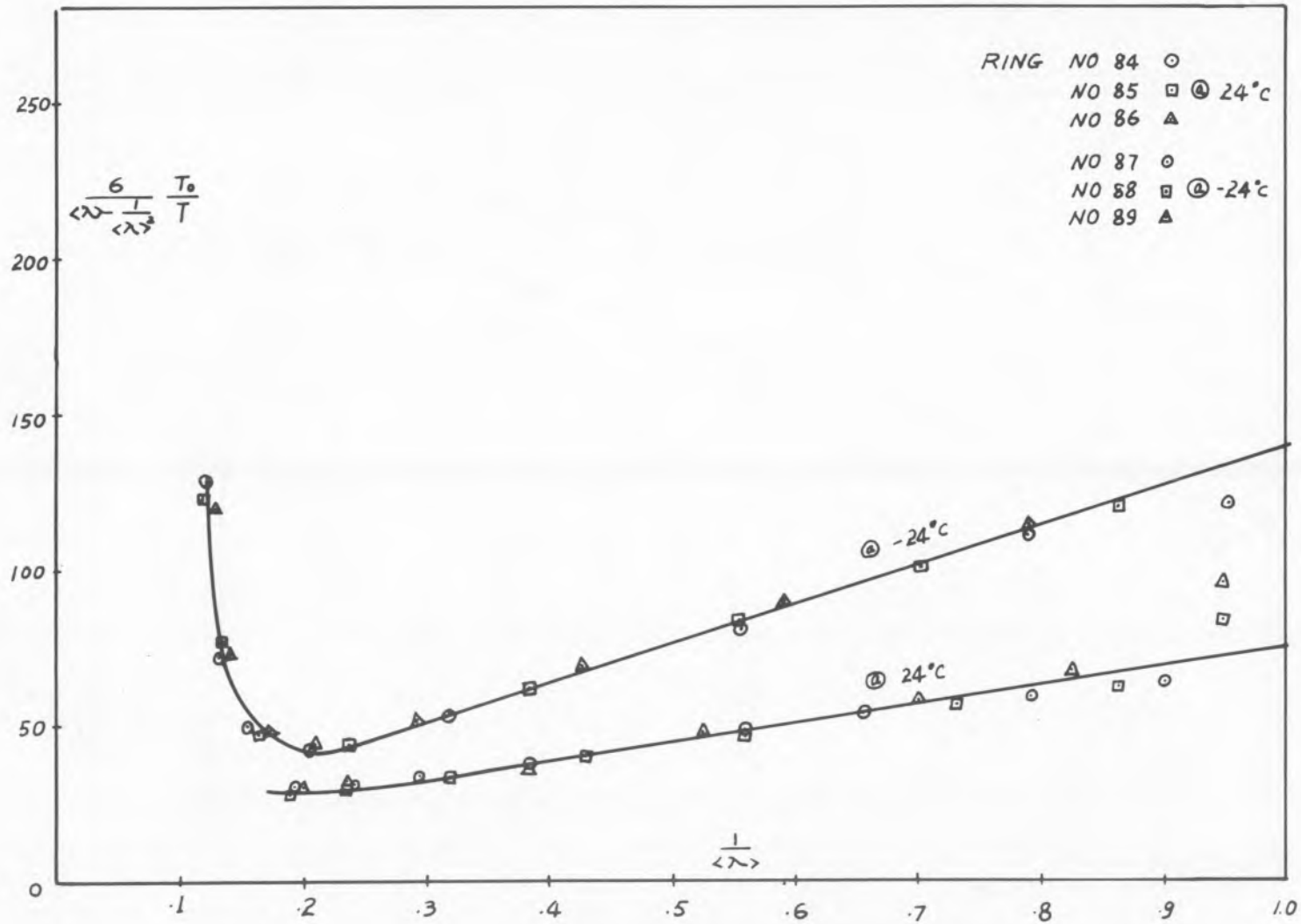

Fig. 14. SBR-MBT-S , ACETONE EXTRACTED

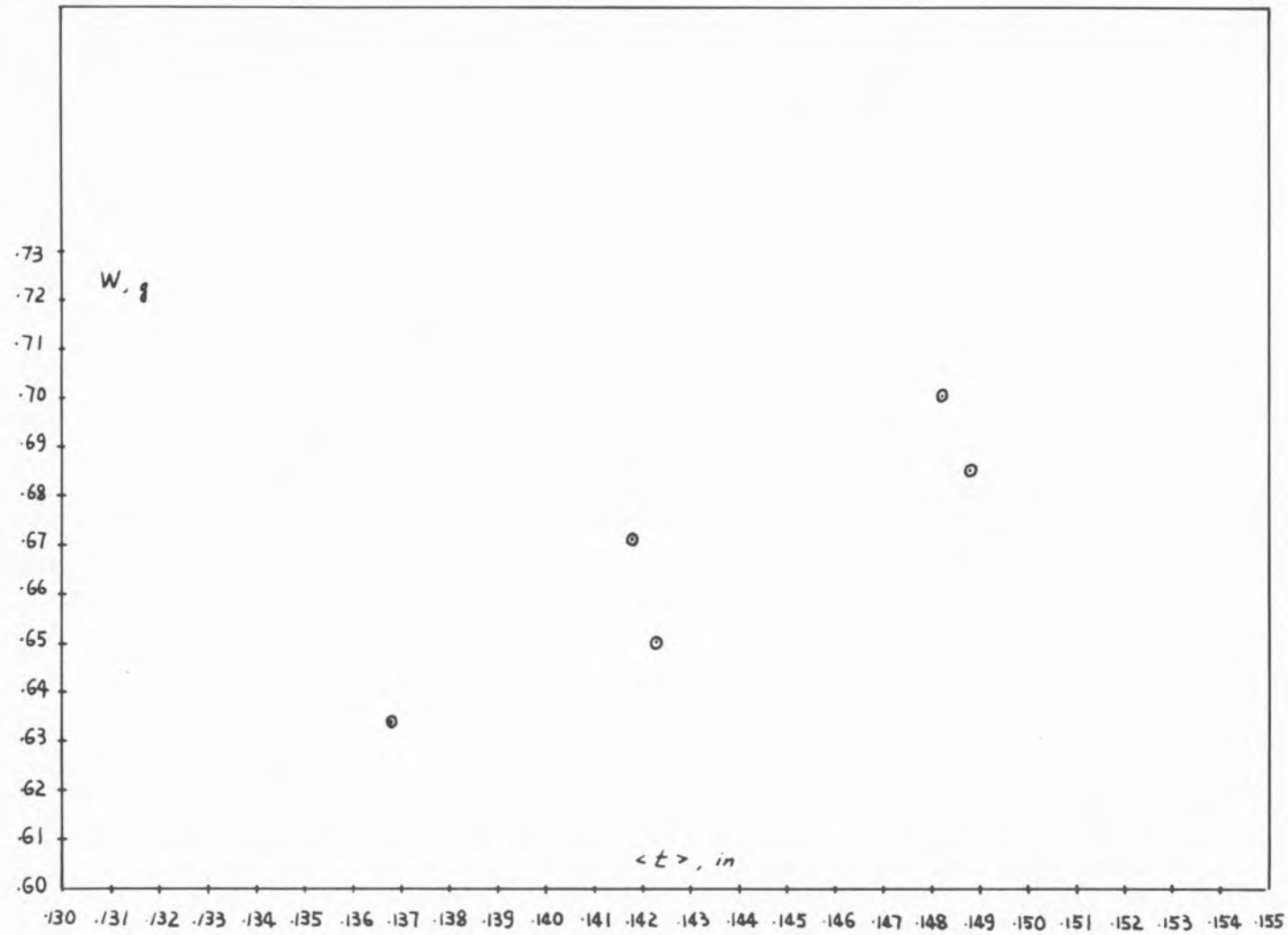

Fig. 15 WEIGHT-THICKNESS CORRELATION FROM TRAVELING MICROSCOPE

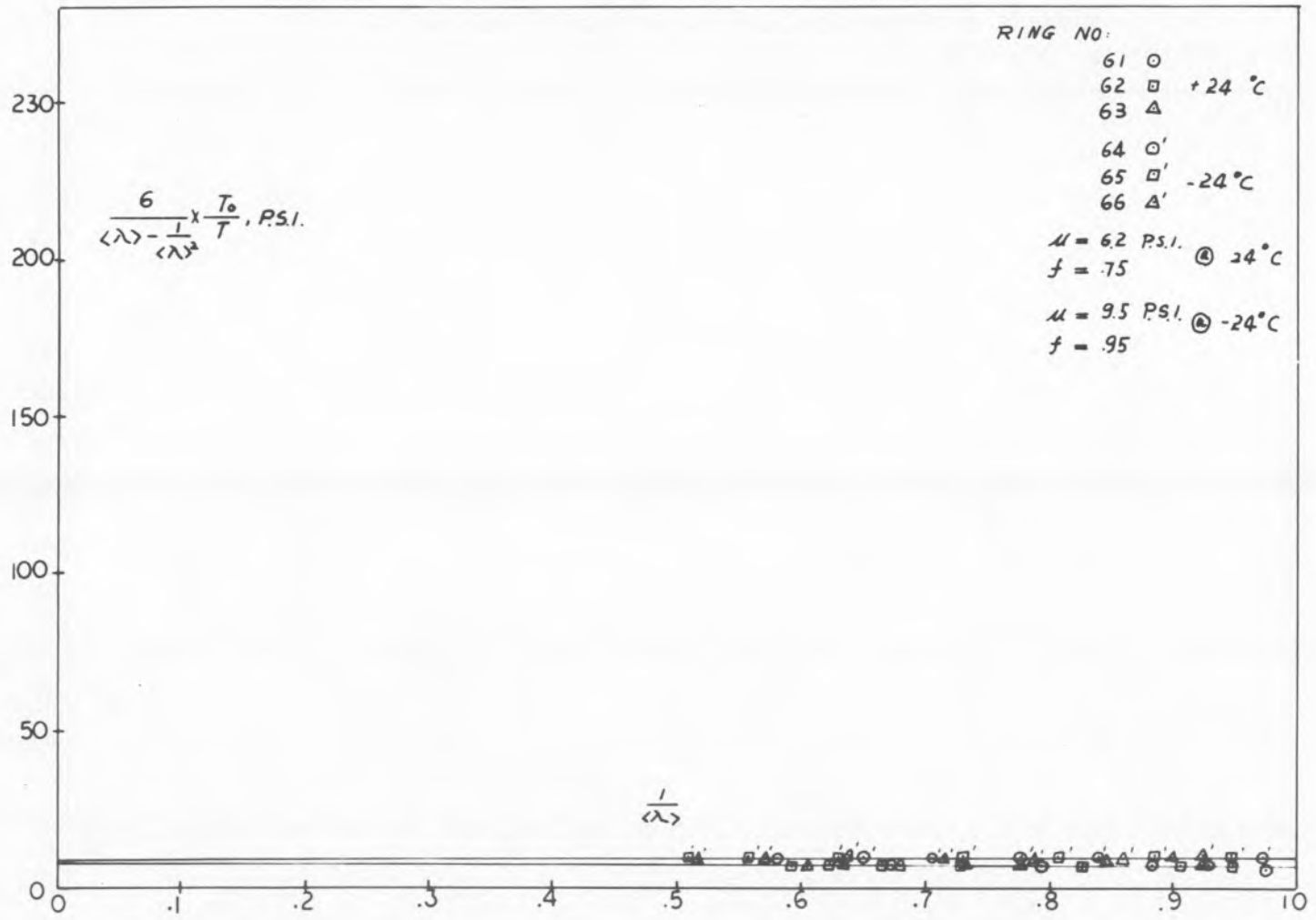

Fig. 16. MOONEY–RIVLIN PLOT FOR SBR-MBTS SWOLLEN IN TOLUENE, AND PULLED AT 1"/MIN DRIPPING WET

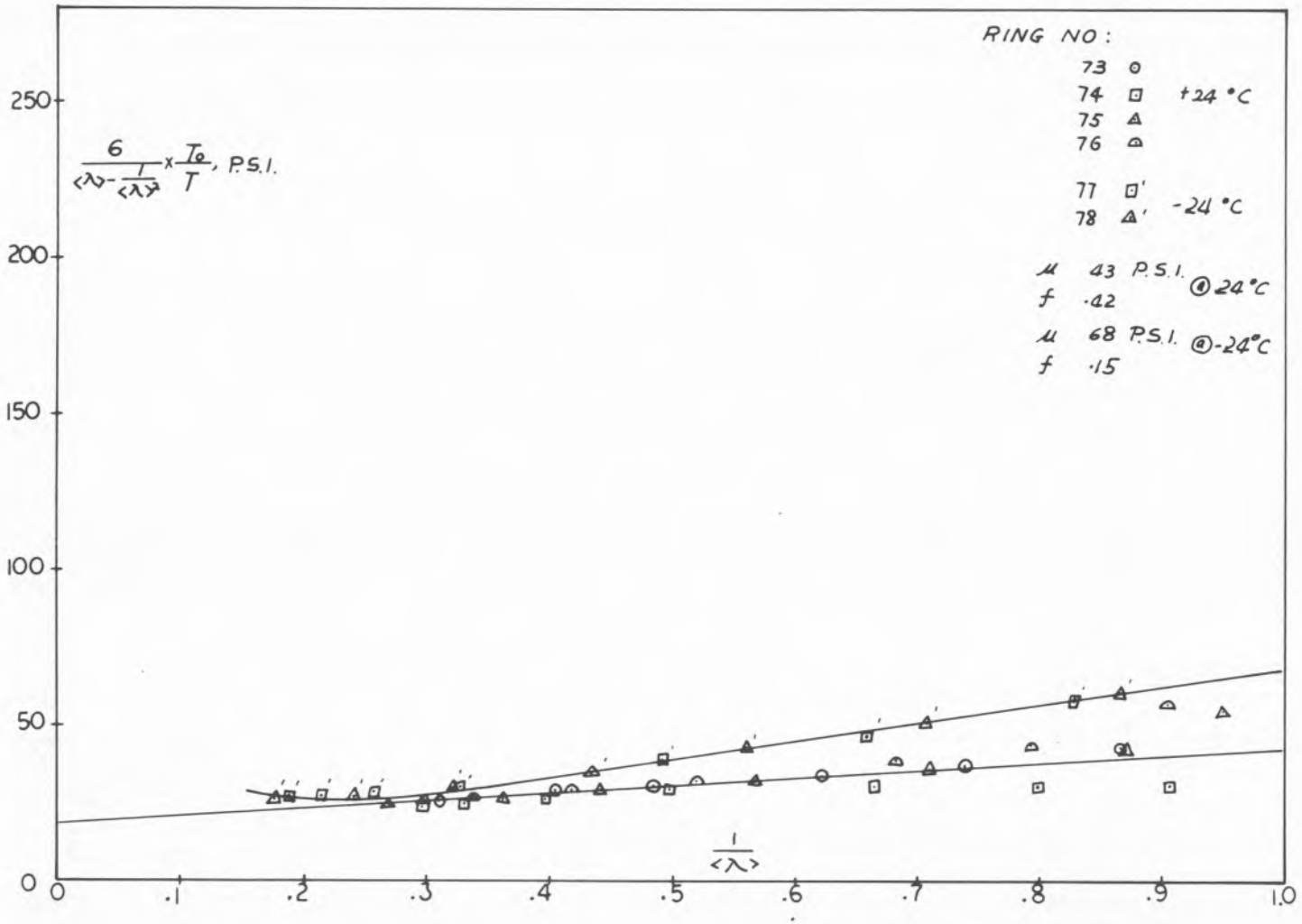

Fig. 17. MOONEY-RIVLIN PLOT FOR SBR-MBTS SWOLLEN IN TOLUENE, VACUUM DRIED, ACETONE EXTRACTED, AND PULLED AT 1"/MIN DRIPPING WET

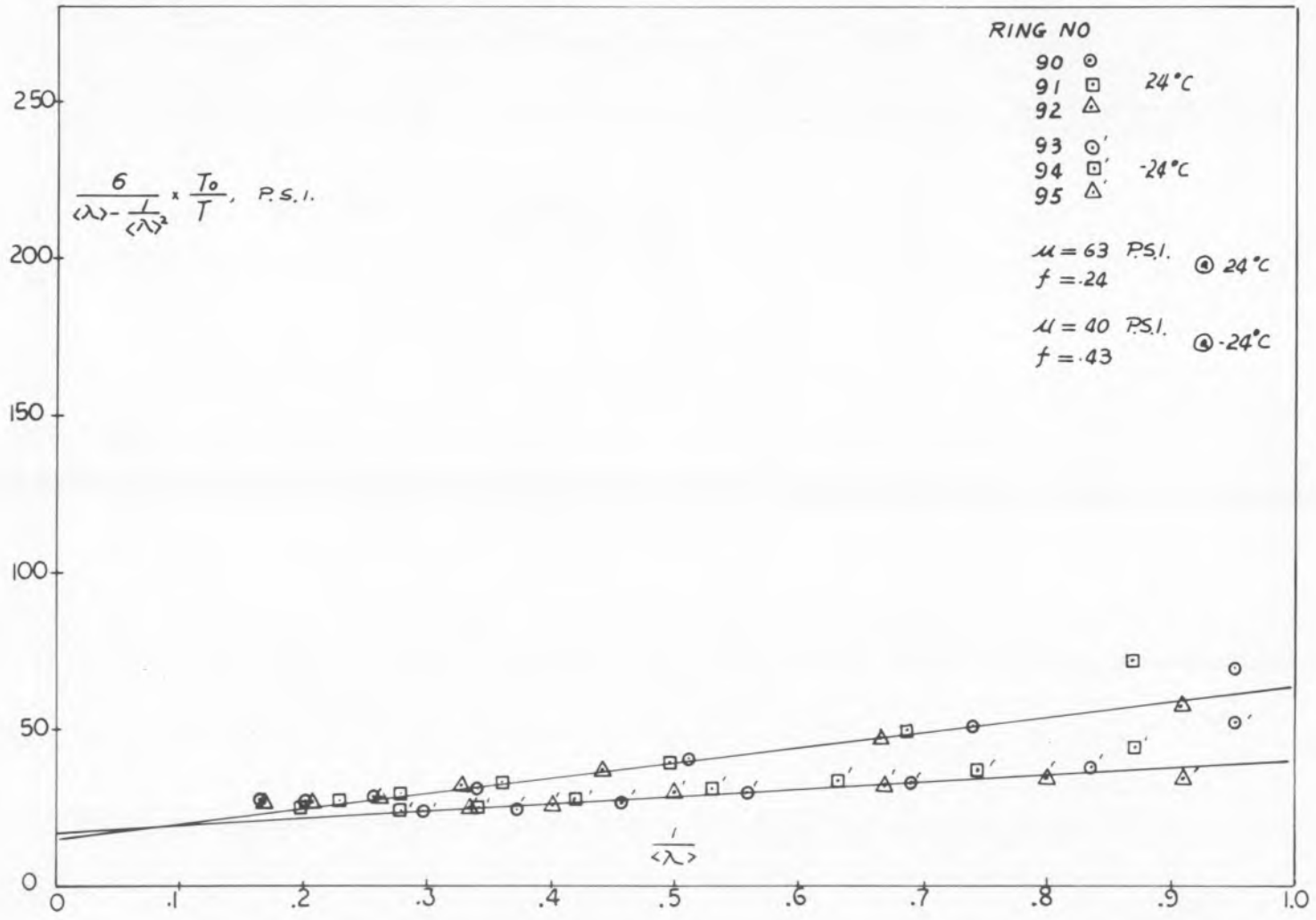

Fig. 18. MOONEY-RIVLIN PLOT FOR SBR-MBTS ACETONE EXTRACTED, AND PULLED DRIPPING WET

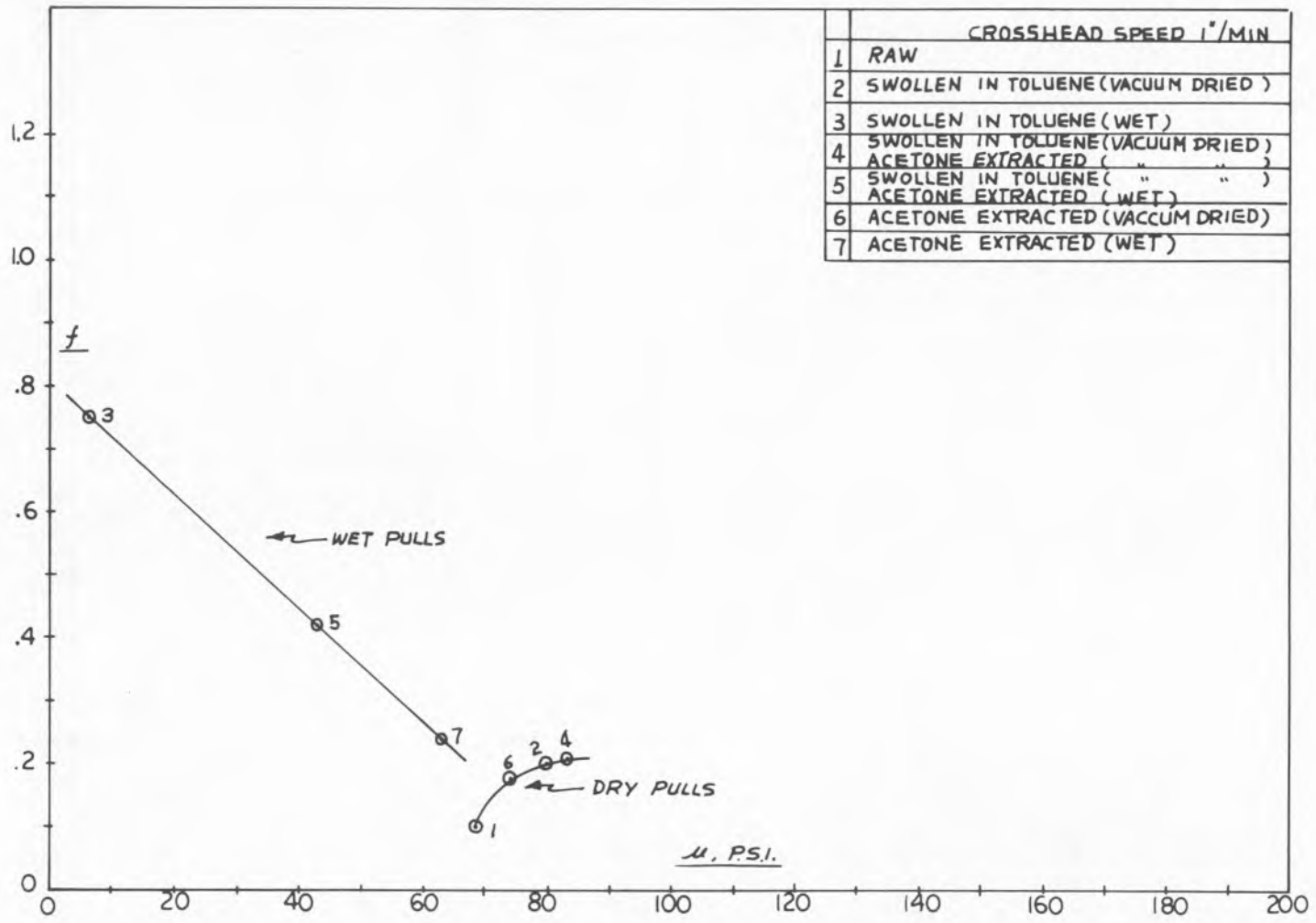

Fig. 19. MOONEY-RIVLIN PARAMETERS AS A FUNCTION OF SOLVENT TREATMENT AT +24 °C

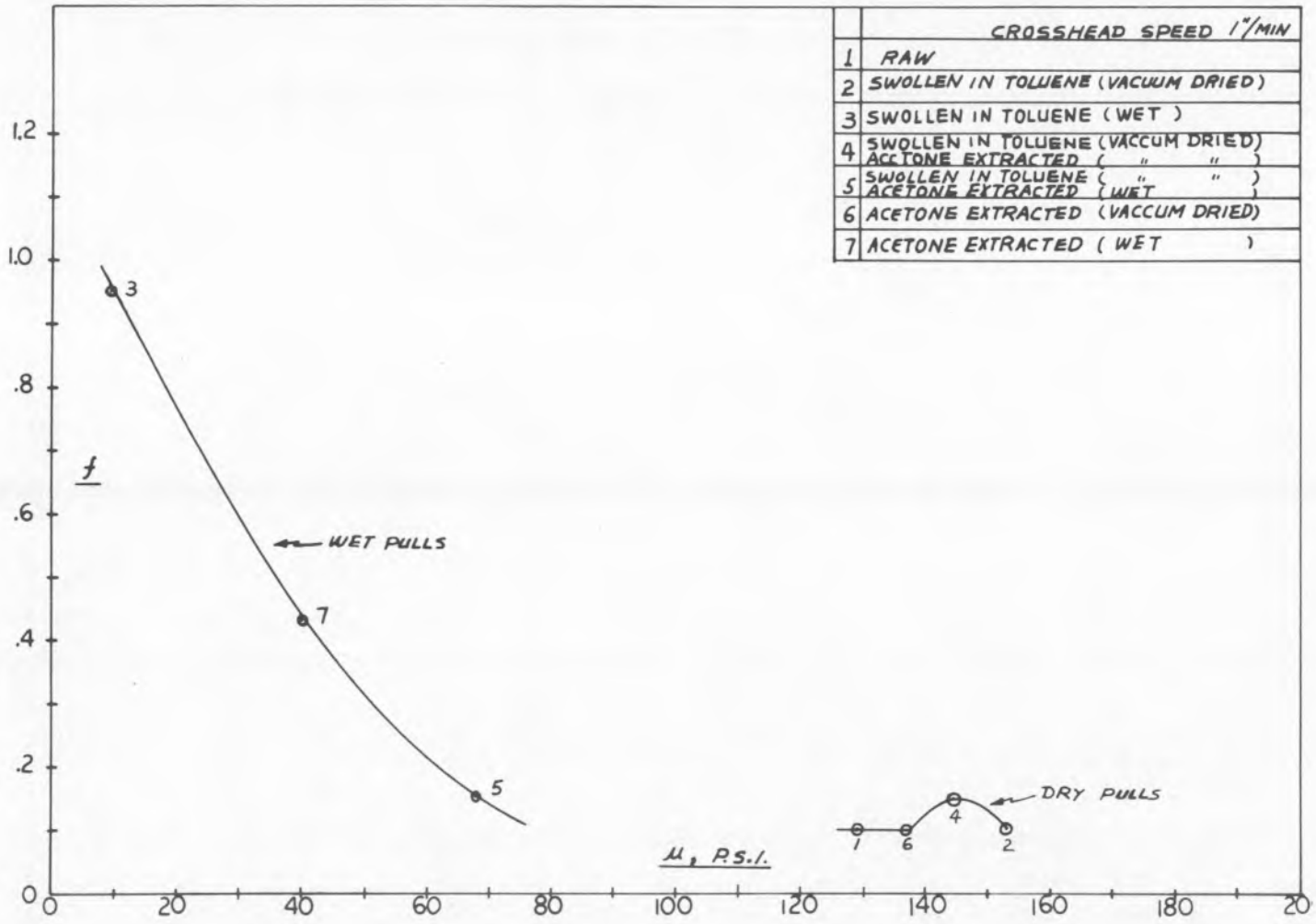

Fig. 20. MOONEY-RIVLIN PARAMETERS AS A FUNCTION OF SOLVENT TREATMENT AT -24°C

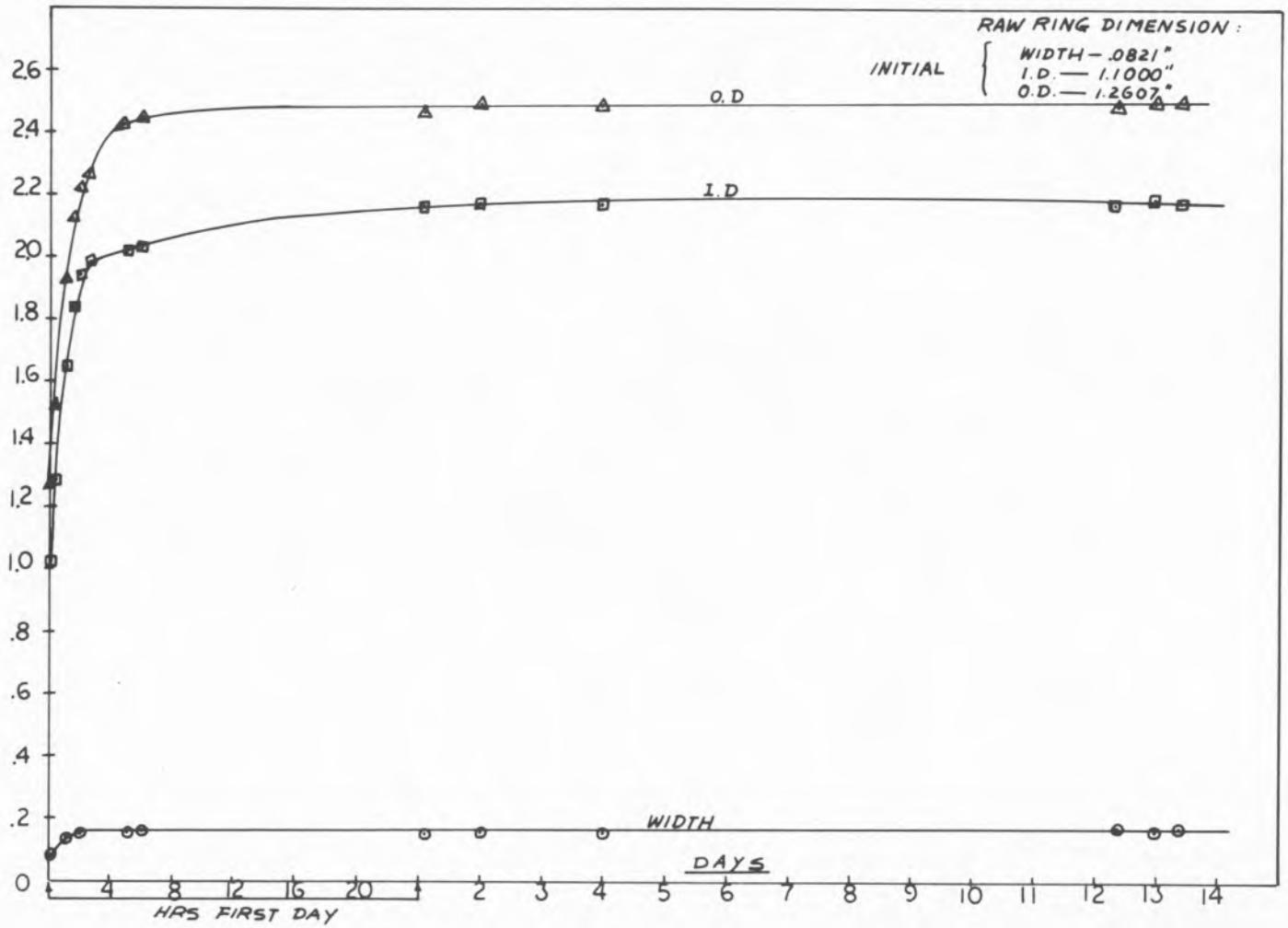

Fig. 21. TIME DEPENDENCE OF SWELLING OF SBR-MBTS RING IN TOLUENE AT ROOM TEMPERATURE

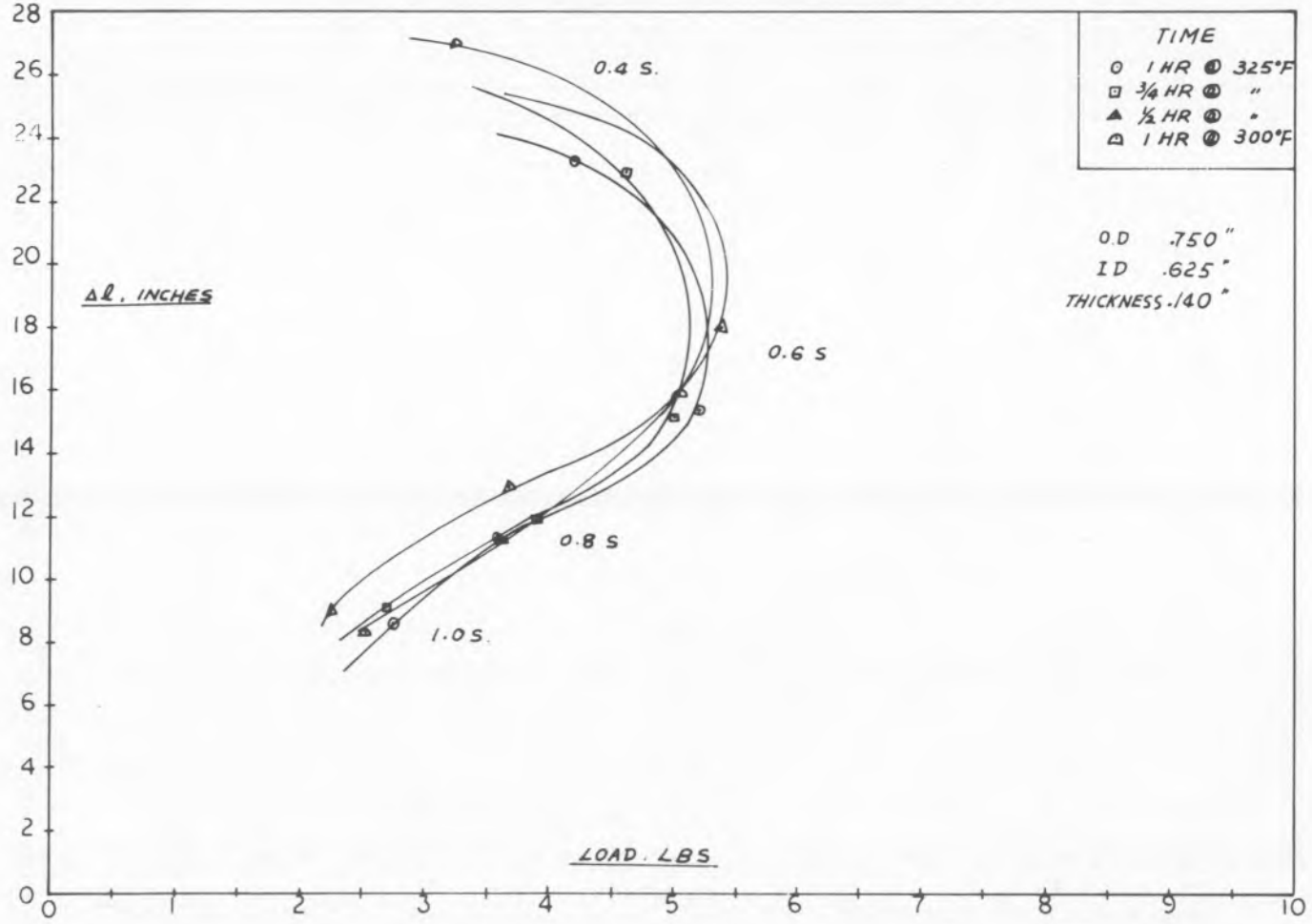

Fig. 22. ULTIMATE PROPERTIES OF PLASTICIZED KAWABATA FORMULATIONS PULLED AT +24°C FOR VARIOUS CURE SCHEDULES & VARIOUS CURATIVE CONCENTRATIONS BASED ON MBT

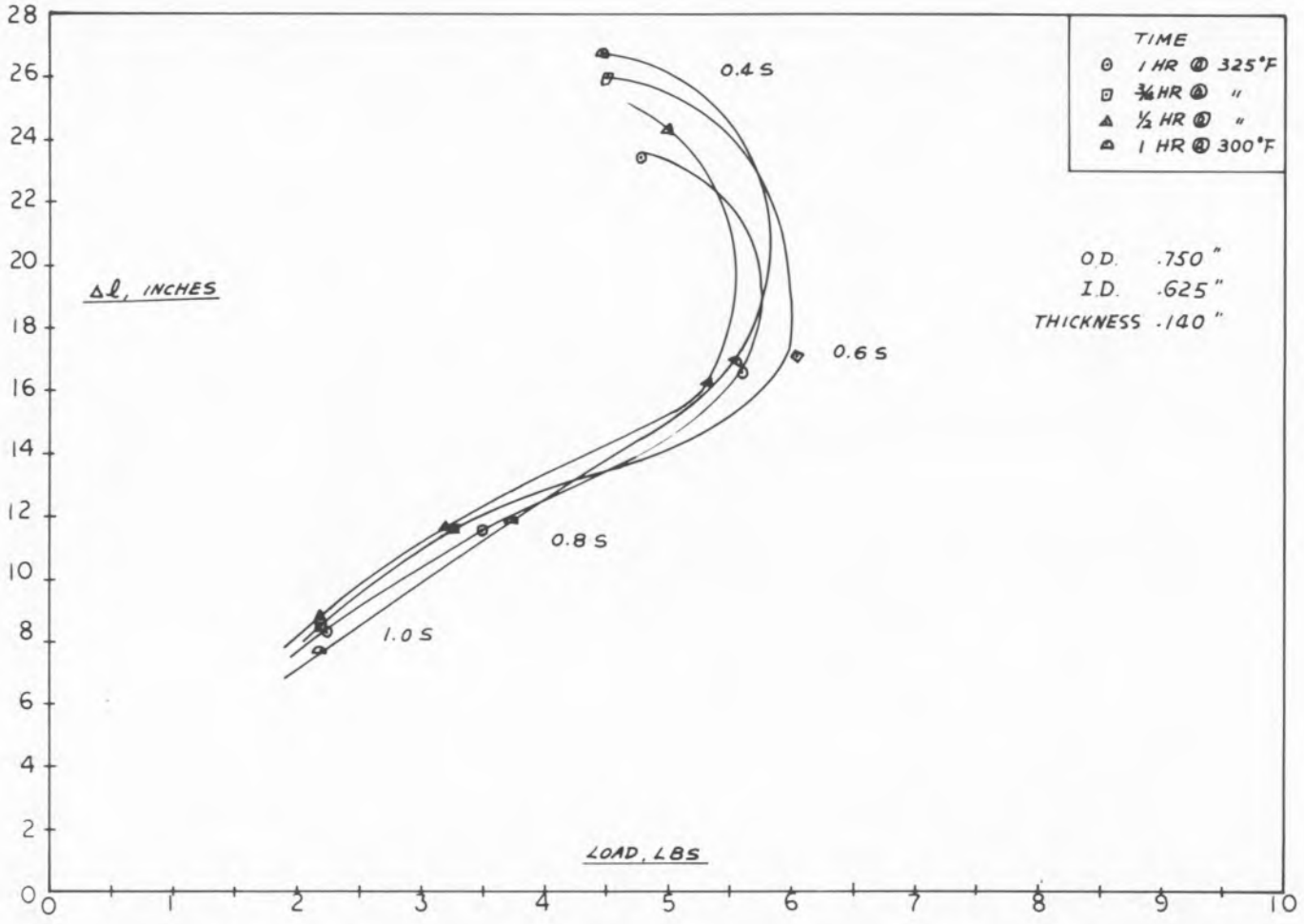

Fig. 23. ULTIMATE PROPERTIES OF PLASTICIZED KAWABATA FORMULATIONS PULLED AT +24°C FOR VARIOUS CURE SCHEDULES AND VARIOUS CURATIVE CONCENTRATIONS BASED ON MBTS

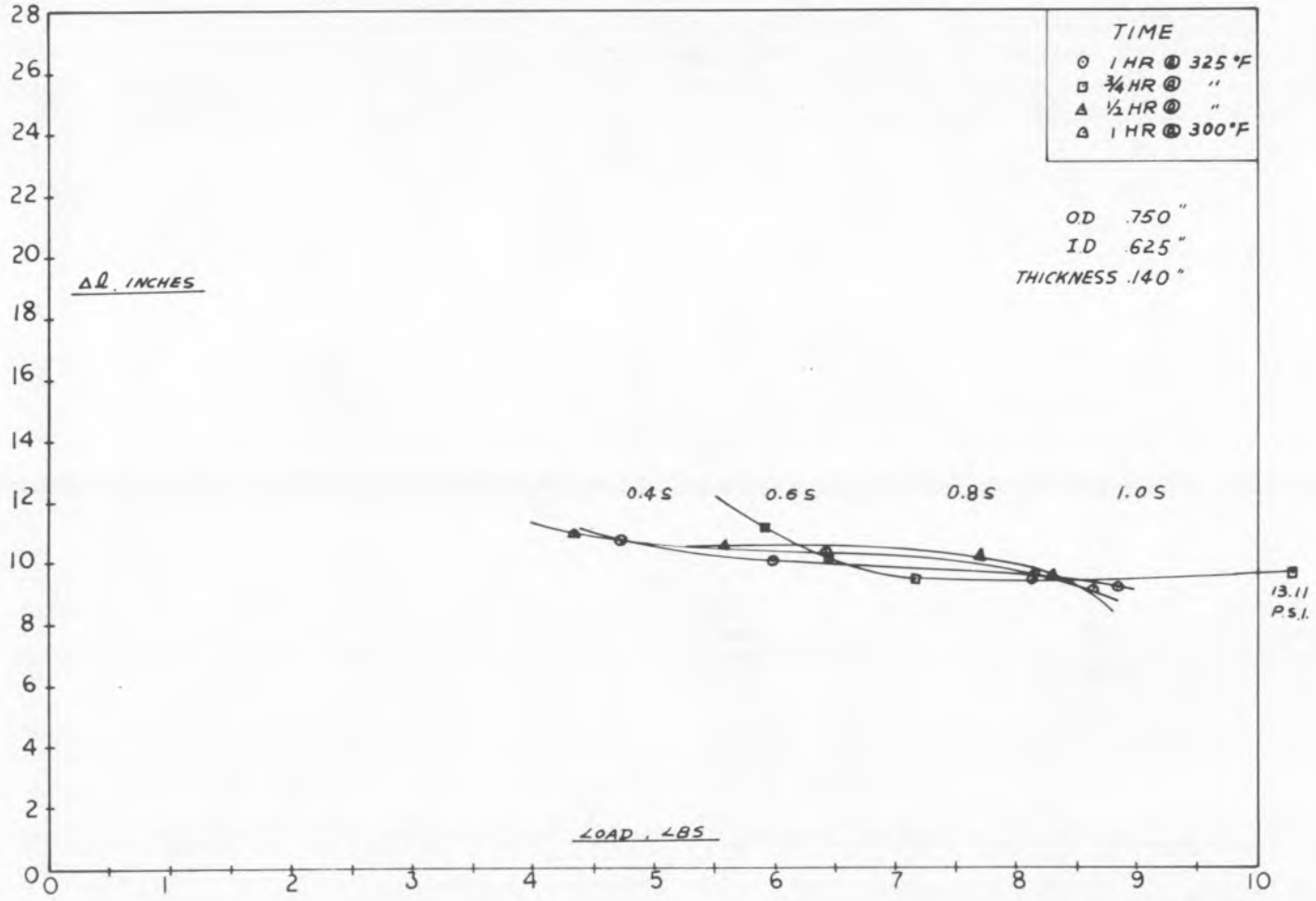

Fig. 24. ULTIMATE PROPERTIES OF PLASTICIZED KAWABATA FORMULATIONS PULLED AT -30°C FOR VARIOUS CURE SCHEDULES AND VARIOUS CURATIVE CONCENTRATIONS BASED ON MBT

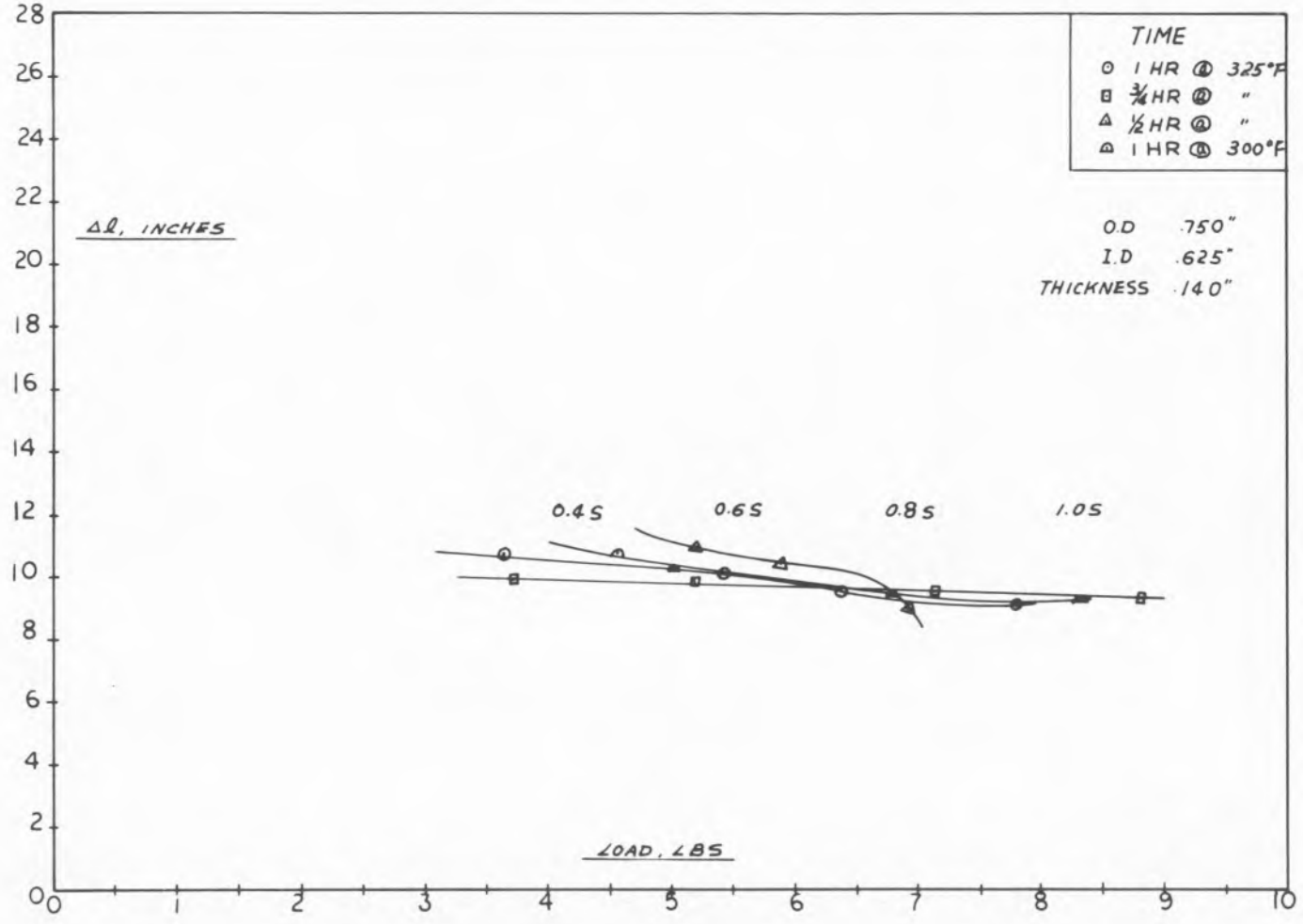

Fig. 25. ULTIMATE PROPERTIES OF PLASTICIZED KAWABATA FORMULATIONS PULLED AT -30°C FOR VARIOUS CURE SCHEDULES & VARIOUS CURATIVE CONCENTRATIONS BASED ON MBTS

TABLE I. Mean Break Time and Crack Growth Rates as a Function of Load

Constant Load, Kg	σ_o, Kg/cm^2	$\langle t_b \rangle$ min	$\sqrt{\frac{\langle t_b^2 \rangle}{\langle t_b \rangle^2} - 1}$	$m_c = \frac{1}{\langle t_b \rangle}$	$m_c = \sqrt{\frac{2}{\langle t_b^2 \rangle}}$	$\langle \lambda_b \rangle$
0.90	7.42	1.213×10^{3}	3.760	8.24×10^{-4}	3.00×10^{-4}	4.06
1.00	8.25	3.853×10^{2}	0.740	2.60×10^{-3}	2.96×10^{-3}	4.60
1.10	9.08	1.293×10^{2}	1.120	7.73×10^{-3}	8.03×10^{-3}	5.03
1.20	9.90	3.369×10^{1}	0.356	2.97×10^{-2}	2.80×10^{-2}	5.46
1.30	10.72	1.363×10^{1}	0.888	7.34×10^{-2}	9.30×10^{-2}	5.86
1.40	11.55	6.237	1.110	1.60×10^{-1}	$1.5. \times 10^{-1}$	6.06
1.50	12.38	2.256	0.747	4.43×10^{-1}	4.40×10^{-1}	6.33

TABLE II

Mooney-Rivlin Parameters for SBR-MBT-S Vulcanizates

A. Shear Moduli, psi

	$T = +24^{\circ}C$	$T = -24^{\circ}C$
Pulled dry	69	129
Swollen in toluene, vacuum dried, pulled dry	80	153
Swollen in toluene, vacuum dried, acetone extracted, pulled dry	83	145
Acetone extracted, pulled dry	74	137
Averages of last three cases ($\pm 1\sigma$)	79 ($\pm$ 4.6)	145 ($\pm$ 8)

B. $f \equiv C_1/\mu$

	$T = +24^{\circ}C$	$T = -24^{\circ}C$
Pulled dry	.10	.10
Swollen in toluene, vacuum dried, pulled dry	.20	.10
Swollen in toluene, vacuum dried, acetone extracted, pulled dry	.21	.15
Acetone extracted, pulled dry	.18	.10
Averages of last three cases ($\pm 1\sigma$)	.197 ($\pm$ .015)	.117 ($\pm$ .029)

DISTRIBUTION

Distribution of this report has been made to all recipients Category 2, Chemical Propulsion Mailing List, March 1965, CPIA Publication No. 74.

Unclassified

Security Classification

DOCUMENT CONTROL DATA - R&D

(Security classification of title, body of abstract and indexing annotation must be entered when the overall report is classified)

1. ORIGINATING ACTIVITY *(Corporate author)*
Air Force Rocket Propulsion Laboratory
Research and Technology Division
Edwards Air Force Base, California

2a. REPORT SECURITY CLASSIFICATION
Unclassified

2b. GROUP

3. REPORT TITLE

PHYSICOMECHANICAL BEHAVIOR OF RUBBERLIKE MATERIALS

4. DESCRIPTIVE NOTES *(Type of report and inclusive dates)*
Second Annual Report - 2 February 1965 to 31 January 1966

5. AUTHOR(S) *(Last name, first name, initial)*

BLATZ, Paul J.

6. REPORT DATE	7a. TOTAL NO. OF PAGES	7b. NO. OF REFS
January 1966	86	20

8a. CONTRACT OR GRANT NO.
AF 04(611)-9572

b. PROJECT NO.
AFSC Project Number 3059

c.
Program Structure Number 750G

d.

9a. ORIGINATOR'S REPORT NUMBER(S)
AFRPL-TR-66-22

9b. OTHER REPORT NO(S) *(Any other numbers that may be assigned this report)*
MATSCIT PS 66-2

10. AVAILABILITY/LIMITATION NOTICES

11. SUPPLEMENTARY NOTES

12. SPONSORING MILITARY ACTIVITY
AFFTC, Directorate of Procurement,
(FTMKR-3)
Edwards AFB, California 93523

13. ABSTRACT

During the past year, further progress was made in understanding both the molecular nature of the strain energy function of a homogeneous, nearly incompressible rubberlike material. The importance of non-affinity of deformation, chain stiffness, and volume exclusion in modifying the basic statistical model of Kuhn, Grün, James and Guth are discussed.

A phenomenological theory for predicting the distribution of times-to-break arising in creep failure in terms of the growth of defects in rubber was proposed and showed good agreement with experimental data.

Batches of thermoelastic rubber filled with glass beads are being prepared prior to evaluation in terms of sedimentation theory.

DD FORM 1 JAN 64 1473 0101-807-6800

Unclassified

Security Classification